Delft University of Technology
Faculty of Electrical Engineering, Mathematics and Computer Science

Bachelor's thesis

Measuring Device for Controlling a Vaporising Liquid Microthruster

July 8, 2019

Proposer / Supervisor:
dr. ing. H.W. van Zeijl

Chair
Nuria Llombart Juan

Authors:
C.A Straathof
R.R. van Wijk

Daily supervisors:
A. Kurmanbay
B. Mansouri

Jury:
Pascal Aubry
Anton Montagne

Abstract

The objective of the project is to design a system which can control the temperature of a vaporizing liquid microthruster (VLM). The liquid in a VLM is heated using a heater resistor. This resistor will be used to both heat the liquid and measure the temperature.
In this thesis the subsystem responsible for the measurements and the conversion of the measured signals to the digital domain will be discussed. We propose a method where short measurement current pulses of a fixed amplitude are applied to the heater resistor. As an optimization, these pulses are omitted when a certain current threshold has been met.
Results show that the system can measure temperature with $\pm 1\,^{\circ}\mathrm{C}$ accuracy, however more full system measurements are required to ensure functionality as a whole.

Preface

This thesis written in the context of the Bachelor Graduation Project. The project was proposed by dr. ing. Henk van Zeijl with the goal to design a data-acquisition/control system for the research of microthrusters.
We would like to express our gratitude to our supervisors dr. ing. Henk van Zeijl and ir. Brahim el Mansouri, and the designer of the thrusters ir. Alister Kurmanbay. We would like to thank ir. Anton Montagne and dr.ir. Chris Verhoeven for their help in the design process, and for allowing us to use their equipment. We would also like to thank ing. Xavier van Rijnsoever and ing. Julius Weinmiller for their time and the feedback they gave at the green-light assessment. Additionally, we would also like to thank dr.ir. Ger de Graaf for lending us the IR-camera. Finally, we would like to thank Koen Lam, Mirza Mrahorovic, Marjolein Rebers and G. Breysens for the cooperation in the project.

Contents

Chapter 1

Introduction

Pico- and nanosatellites have increased in popularity over the years [1]. Figure 1.1 shows the increase of nanosatellites launches of the past years and the predicted exponential increase for the upcoming years. Nanosatellites can be used in a wide variety of fields, such as space debris removal [2], formation flying [3] or swarm missions [4]. They are lightweight and low-cost, but usually lack propulsion capability. There is still much research to be done into the micro-propulsion system for these satellites. The need for further development of these systems is also mentioned in the technology roadmap set by NASA [5].

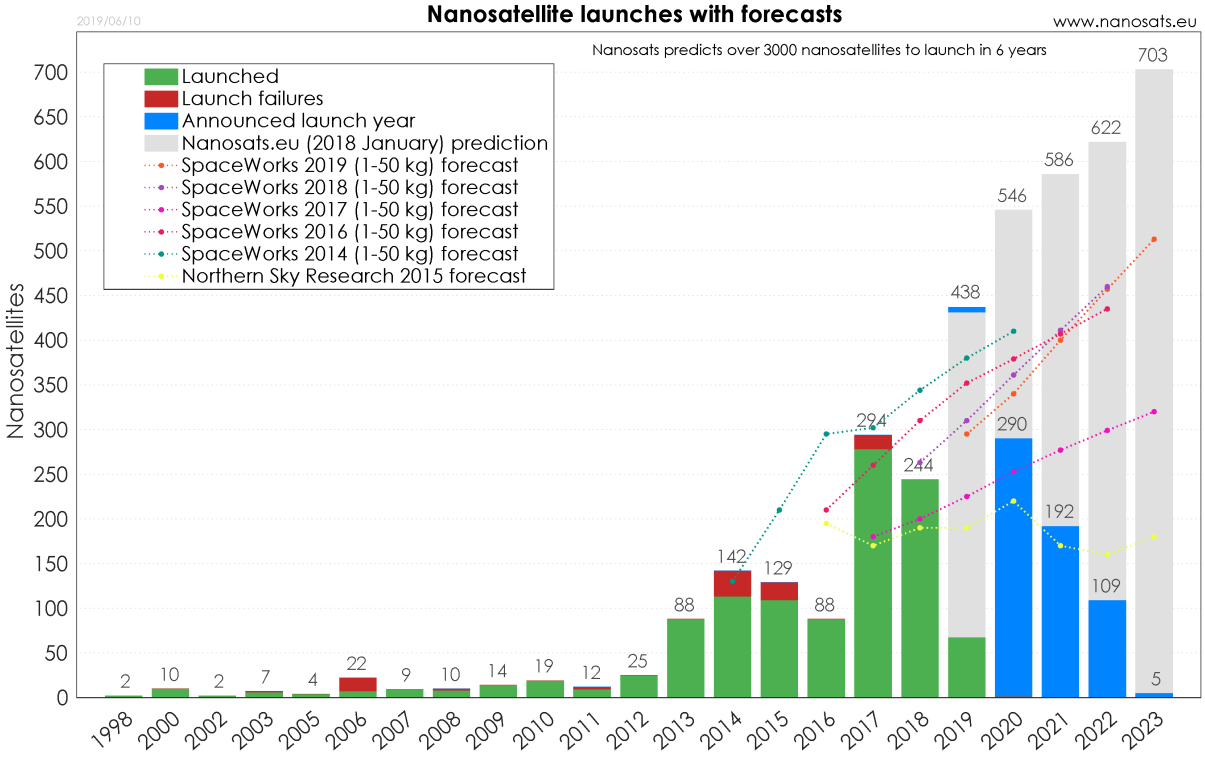

Figure 1.1: Nanosatellites launches from the past and a prediction for the coming years from [6]

1.1 Background information

Micro-propulsion systems have many different variations based on their working principle, ranging from solar sails, cold gas propulsion systems, electric propulsion systems and chemical

propulsion systems [7]. This project focuses on the resistojet thruster, which falls in the category of electric propulsion systems. There are in general two main types of microresistojets: the vaporizing liquid microthruster (VLM) and low-pressure microresistojet (LPM) [8]. In this project, we work with a VLM that is supplied by our supervisor and which is developed within a research project.

A VLM generally consists of a resistive heating element and a liquid channel, as shown in Figure 1.2. Thrust is delivered by heating a gas or liquid, accelerating it through a nozzle and expelling it into space. In our case, the propellant is water. When the water is heated up and starts to boil, bubbles appear inside the channel. These bubbles form a layer of thermal insulation and affect the heat transfer from the heater to the channel. This in turn affects the temperature of the resistive element and the pressure in the channel. Therefore, the amount of steam generated tend to oscillate. As the thrust is dependent on the mass flow rate [9], unwanted variations in the temperature and pressure can therefore lead to a fluctuating thrust. Furthermore, uncontrolled heating could even cause thermal runaway and destroy the device. Therefore, controlling the temperature of the heater element is of paramount importance.

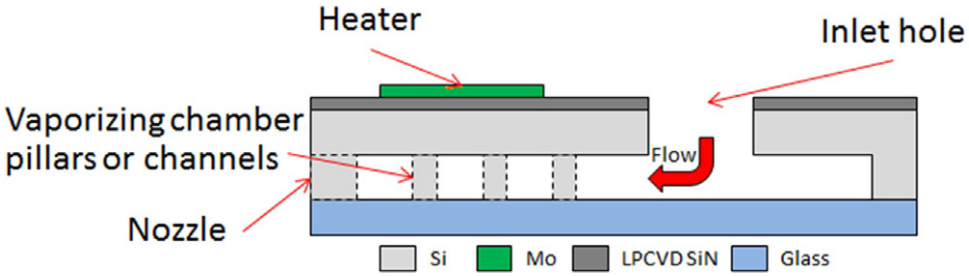

Figure 1.2: Schematic cross-section of the thruster taken from [9]

1.2 State-of-the-Art Analysis

Small satellites like CubeSats have several constraints that form a limitation in the design. Examples of these factors are its mass, dimensions, available power and propulsion [10]. Hence there is a need for high performance, highly miniaturized and integrated micro-propulsion systems that meet these constraints [11].

Tummala and Dutta compared different micro-propulsion systems for CubeSats [12]. Their research shows that resistojets provide a relatively low specific impulse, have the highest average thrust-to-power ratio compared to other electric propulsion systems and can deliver a thrust between 0.1 mN and about 50 mN. This relatively low thrust can also be seen in the microresistojet propulsion concepts from Cervone, Zandbergen, Guerrieri, De Athayde Costa e Silva, Krusharev, and Zeijl [13]. In this work, they state that the presented concepts have the most potential in nanosatellite applications in which a thrust between 0.5 mN and 10 mN is required. Due to their relatively low thrust, resistojets are also used on larger satellites for attitude control [12].

Controlling the thrust in magnitude and direction could make a big difference in the use of micro-propulsion systems [13]. A possible solution to control the thrust magnitude is to control the mass flow rate with micro-pumps [14] [15].

Another possible solution to control the thrust is to reduce bubble forming during heating. The transient behavior of bubble formation on micro-resistors is an active field of study [16]. Tsai and Lin have observed that the temperature of the heater rises with the increase of bubble size to reach a new equilibrium temperature, because it is believed that the heat dissipation path from the micro resistor surface to the liquid is partially blocked by the vapor bubble. Several experiments have also been performed on microheaters to better understand the boiling

process [17]. Our project will be an attempt to control the temperature of the microheater and thereby also to control the bubbling process.

1.3 Project Objective

In an attempt to stabilize the thrust, we have defined the following goals for the project:

1. To study the dynamic liquid/vapor phenomenon by acquiring data about the temperature of the heating element.

2. To control the temperature of the heating element in an effort to reduce bubble forming.

These two goals are the highest priority for the project. Besides these goals, a third goal is also set. However, this goal has less priority than the first two goals.

3. To study the dynamic liquid/vapor phenomenon by acquiring data about the pressure in the channel.

To achieve these goals, we implement the required hardware and software compatible with this device. The resistojet thruster that we work with can be found in the Appendix. The heater element and pressure sensors are integrated into the device.

The microthruster is supposed to work in space on nanosatellites. However, this project is part of a research project on manufacturing microthrusters. Therefore, we assume that our system is only going to work on earth as a first prototype. Phenomena such as space radiation, high pressure and extreme temperature variations will be omitted and constraints such as limited space, limited power and extreme robustness will not be given priority in the design. This simplifies the design while providing valuable information to reach the objectives of the project.

The project can be considered a success if the following deliverables are accomplished.

1. Design and implementation of a breadboard (or PCB) with circuitry for real-time data acquisition from heater (RTD) array and from multiple EPCOS pressure sensors.

2. Design of Front end data acquisition software.

The results obtained from this project enable researchers to further investigate the effect of the bubble forming in microthrusters.

1.4 Subdivision of project

In order to reach the objectives of the project, the project is divided into subgroups.

The temperature of the heater device is affected by supplying an electric input signal to the heater. The accuracy of this input signal determines the precision of the temperature which can be set. This is the challenge of the first subgroup: the supply group.

Implementing a feedback system poses some challenges, as there is no model available of the microthruster. Furthermore, effects such as the heat dissipation and stochastic bubble forming makes modelling even more complex. Nonetheless, the need for an adequate feedback system is of uttermost importance for controlling the temperature. This is the focus of the another subgroup: the control group.

Providing reliable input to the feedback system means that the resistance of the heater element should be read out accurately. The temperature dependence makes this a challenging task. Therefore, another subgroup is formed which tackles this challenge: the read-out subgroup.

A high level overview of the system is given in Figure 1.3. To summarize, the following three subgroups are formed.

- Control: responsible for the control of the system.
- Read-out: responsible for the hardware read-out circuitry.
- Supply: responsible for the supply for the heater.

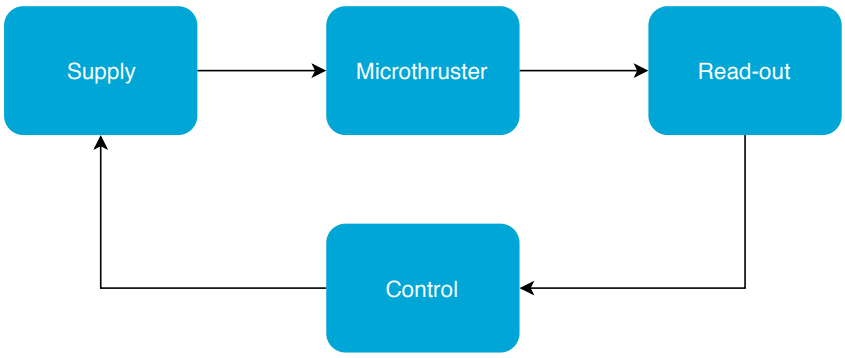

Figure 1.3: Overview of the subgroups

1.5 Readout Group Specific

1.5.1 Problem Scope

Our goal is to provide a circuit that facilitates the measurements of voltage, current and pressure. A microcontroller must be able to sample and process this data. The microcontroller itself is outside of the scope of our project: we only design and implement the circuitry to translate physical quantities into the digital domain.

1.5.2 Technical Review

Microthrusters are a subject currently under extensive research. Our project does not focus on the microthruster specifics and behaviour. Instead, our project is about the design of sensor circuits, a topic which is covered extensively and is a core part of electrical engineering. Microthrusters with integrated temperature sensors exist in literature [18, 19]. However, one of our requirements states that the heater must also be used as a sensor. This gives us a very different design constraints compared to a system with a separate sensor.
In [20] a heater design is proposed which uses its own resistance as temperature sensor. Short voltage pulses are sent through the system, and with the measured current, the temperature is estimated. Depending on the conductive material used, the relation between temperature and resistance can be almost linear [21]. The same principle is used in PTC/NTC temperature sensors [22]. Gas chromatography is another field where an integrated heater/sensor can be applied. This is proposed in [23]. As noted, this design limits overshoot caused by the delayed response from the sensor to the varying temperature of the heating element.

1.6 Thesis synopsis

This thesis is divided in several chapters. First, in chapter 2, the requirements of the system are discussed. These requirements are molded into a design in chapter 3. Our considerations, trade-offs and decisions are detailed here. In chapter 4 the component choices and noise calculations are listed. Additionally, our PCB design is documented here. Chapter 5 contains our measurement results and discussion about these results. Next, in chapter 6 conclusions are drawn from these result in comparison with the requirements. Recommendations and future work is outlined in chapter 7. Finally, our appendices are at the very end of this document.

Chapter 2

Program of Requirements

The goal of the project is to design and implement a system which controls the temperature of the heater element in a resistojet and provides temperature and pressure readings.

We have grouped the requirements of the system into several categories. Functional requirements describe what the system must have. The system requirements are limitations of the system and the safety requirements are set to prevent that the system damages its environment. Lastly, the implementation requirement describes how the system should be built. The requirements can be found below. We have distinguished mandatory requirements (MR) from trade-off requirements (ToR).

Functional requirements

1. The temperature read-out must have an accuracy of $\pm 1\,^{\circ}\mathrm{C}$. [MR]
2. The temperature control must be within $\pm 10\,^{\circ}\mathrm{C}$ of the set-point. [MR]
3. The resistor must be used as the heater. [MR]
4. The resistor must be used as the sensor. [MR]
5. The temperature of the load should not be affected by a temperature measurement [MR]
6. The measurement needs to be a 4-probe measurement. [MR]
7. The system must have front-end data acquisition software. [MR]
8. At least two EPCOS pressure sensors need to be read out. [ToR]
9. The system should preferably read out at least three thrusters. [ToR]

Safety requirements

1. The maximum temperature should not exceed 300 °C [MR]
   degree Celsius; the temperature should not become higher.

System requirements

1. The circuit has to be portable. [MR]
2. The system should not use more than 10 W. [ToR]
3. The system should be able to be connected to different loads (i.e. thrusters) ranging from 100 to 1000 Ω. [ToR]

Implementation requirement

1. The system should preferably be implemented on a PCB. [ToR]

Chapter 3

Design

3.1 Introduction

In order to estimate the temperature of the heating element, we need to determine its resistance. To achieve this, the voltage and current need to be measured. For the molybdenum heater resistor, the correlation between temperature and resistance can be approximated with the following equation [2]:

$$\begin{aligned} R(T) &= R_0 \left[1 + \alpha(T - T_0)\right] && (3.1) \\ &= R_0 + \alpha R_0 (T - T_0) \\ &= \underbrace{R_0 - \alpha R_0 T_0}_{\text{constant}} + \underbrace{\alpha R_0 T}_{\text{variable}} && (3.2) \end{aligned}$$

where T is the temperature of the resistor in kelvin, R_0 is the resistance at temperature T_0 in Ohm and α is the temperature coëfficient of the material. α and R_0 are dependent on the resistor used. From our requirements, the resolution should be $T_{res} = 1°\text{C}$. According to Equation 3.2, this gives a difference in resistance equal to $\Delta R = \alpha R_0 T_{res}$. Resistance can however not be measured directly, but can be determined by dividing voltage by current. With Ohm's law and Equation 3.2, one can find:

$$\begin{aligned} V(T) &= I \cdot R(T) \\ &= I \cdot R_0 \left[1 + \alpha(T - T_0)\right] \\ &= I \cdot (R_0 - \alpha R_0 T_0) + I \cdot (\alpha R_0 T) && (3.3) \end{aligned}$$

This gives us the minimal voltage step size:

$$V_{min} = V(T + T_{res}) - V(T) = I \alpha R_0 T_{res} \tag{3.4}$$

which is not only dependent on the temperature, but also on the current delivered to the resistor. How the current level is chosen will be explained later in this chapter.

3.2 Measurement Method

Since our system has to be a controllable current source, the current through the resistor is known. The voltage over the load resistor can be measured. The required accuracy of the voltage measurement depends on the measurement current, thus the measurement current needs to be chosen wisely.

3.2.1 Direct Measurement

The simplest way to measure the temperature is to directly measure the voltage over the heater produced by the heating current. This method can be implemented with a slower current source and ADC, since there are no fast changing signals in this system. The main issue, this method suffers from, is its accuracy. In order to be able to measure every voltage level, one would need to scale the full range into the ADC range. Resistance is what we want to measure, but voltage is measured instead. However, this voltage is also dependant on the input, the current, according to Equation 3.3. Accordingly, the minimal voltage step size given in Equation 3.4 is no longer a fixed value, but changes during operation. Therefore, with a small input current, a very small step size is needed. This reduces the accuracy of the measurements, thus requiring you to use an ADC with a very high resolution, and to set a minimum current. This method puts strong limitations on which hardware you can use, making it less optimal to use.

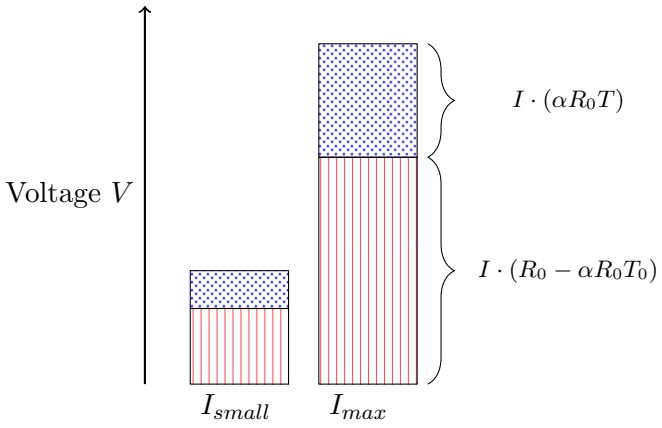

Figure 3.1: Illustration of the resolution issue with the direct method: the voltage across the resistor consists out of two components: The first component (red, vertical lines) only depends on the current, while the second component (blue, dotted) also depends on the actual temperature of the heater.

3.2.2 Time-domain Separation

An improved version of the direct measurement method uses time based separation of heating and measurement signals. This method was found in [20]. Short measurement pulses of a fixed amplitude are sent through the heater periodically. The implementation of this method is still relatively simple, but does have higher speed requirements on the current source and ADCs. The higher speed requirement for the current source is due to the time required for the current to stabilise within N bits of accuracy. This together with the ADC sampling time needs to be fast so the length of the measurement pulses can be reduced. If the measurement pulses are too long, they would affect the temperature of the heater resistor. Furthermore, pulses have in theory unlimited bandwidth. With low-pass filters, this could cause Intersymbol Interference (ISI), where the previous output overlaps with the measurement pulse. One could increase the bandwidth, however this in turn increases noise.

3.2.3 Frequency-domain Separation

Another method to separate the measurement signal from the heating current is by having the two signals at different frequencies. The heating current can be a DC current, and the measurement current can be an AC current. The voltage resulting from this measurement current can be separated from the voltage created by the DC heating current by using a high pass filter. This AC current can have a fixed amplitude. That way the ADC range can be

optimally used. Using this method also has the benefit of having continuous measurements, since the measurement current is always there. This solution is more complicated to implement, since it requires a lot more data processing. The scenario where the heating current makes a large step is also a problem, since this will result in a large voltage spike on the output of the high pass filter. A form of over-voltage protection is needed to prevent these spikes from damaging a buffer opamp or ADC.

3.2.4 Time-Direct Hybrid

If the used ADCs have more resolution than the 9 bits that are required, smaller measurement currents are possible. It is also possible to optimise the measurement method. The proposed measurement method is a hybrid between the direct measurement and the pulse based measurement. If the heating current is above a certain threshold which still allows the measurement to meet the resolution requirement, then the measurement can be done directly. If the heating current is below the threshold, where its is not possible to measure the voltage with sufficient accuracy, a measurement pulse can be sent. This removes the effect of the measurement current on the temperature for a range of heating currents, while keeping the measurements accurate when the heating current is low.

3.2.5 Comparison

In Table 3.1 a short summary of the advantages and disadvantages of each method can be found. Since the direct measurement method requires an impractically large ADC range to measure accurately at low heating currents, it is not a viable method to implement in the system. The method based on time-domain separation wont give the same quality of measurements as frequency domain separated measurements, but the quality should still be sufficient. In implementation the time-domain separation based method is also simpler compared to the frequency-domain separation based method, at the cost of a higher speed requirement for the current source. The method based on time-domain separation is preferred due to its simplicity in implementation, without having large disadvantages like the direct method does.

Method	Advantages	Disadvantages
Direct measurement	- Simple implementation - Low speed requirement	- Very high resolution requirement - Non-optimal use of the ADC range
Time-domain separation	- Simple implementation - Independent of heating current	- High speed requirement - Measurement pulses can affect temperature
Frequency-domain Separation	- Continuous measurements - Average speed requirement	- Complex implementation - High voltage spikes
Time-Direct Hybrid	- Simple implementation - Good use of ADC range	- High speed requirement

Table 3.1: Advantages and disadvantages of the different measurement methods

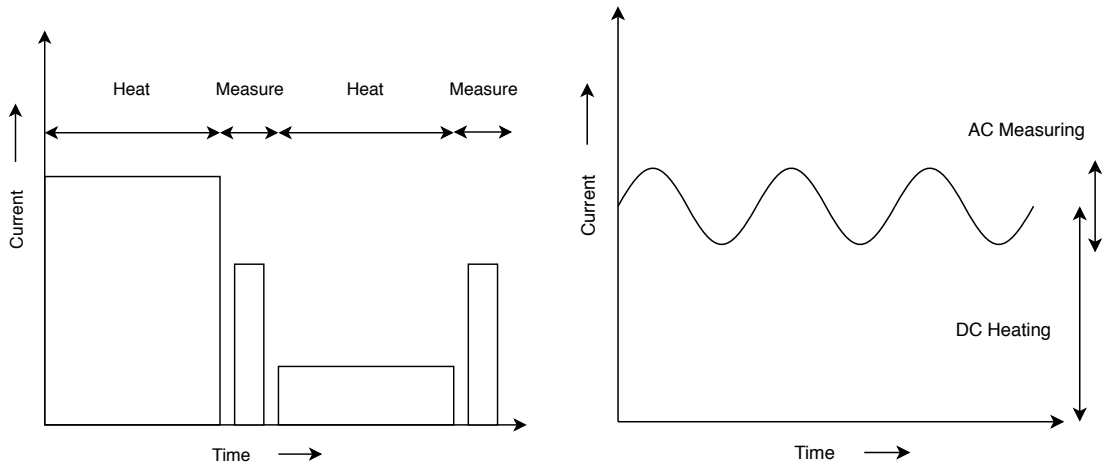

(a) Time-domain separation

(b) Frequency-domain separation

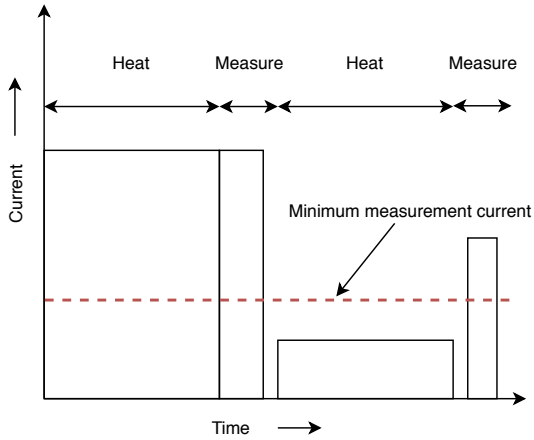

(c) Time-Direct hybrid

Figure 3.2: Schematic overview of the different measurement methods

3.3 Measurement Current

The measurement current is an important parameter when the accuracy of the system is concerned. The maximum value of the measurement current is determined by the supply voltage of the current source, the temperature coefficient, and the temperature range. Equation 3.5 describes the maximum measurement current.

$$I_{max} = \frac{V_{supply}}{R_0 \cdot [1 + \alpha \cdot (T_{max} - T_0)]} \tag{3.5}$$

The minimum measurement current is determined by the temperature requirement, R_0 of the resistor, the temperature coefficient of the heater, the resolution of the ADC that is used for the voltage measurement and the supply voltage. Equation 3.6 describes the minimum measurement current.

$$I_{min} = \frac{V_{supply}}{2^N \alpha T_{res} \cdot R_0} \tag{3.6}$$

3.4 Voltage Measurement

3.4.1 Resistive Dividers

The heater resistor is connected with one side to the voltage supply, and with the other side to the drain of a MOSFET which controls the current through the resistor. Since both ends of the resistor are not grounded, a differential measurement is needed. This can be done with a differential amplifier, or with an ADC that has differential inputs. The voltages to be measured will be in the range of 0 to 70 V, Thus requiring attenuation before being read by the ADC. The easiest way to attenuate a signal is by using a resistive divider, as seen in Figure 3.3. This resistive divider will draw a current which is not an issue at the supply side. However at the side of the resistor which the MOSFET is connected to, this current can be problematic. Three solutions are available to combat this current: To use a divider with a total impedance bigger than 70 MΩ, to put a buffer opamp on the MOSFET side of the resistor, or to compensate for the current in the micro-controller. However, opamps with an input voltage range of over 70V are quite rare and expensive. Using a divider with an impedance of 70 MΩ will introduce a lot of noise to the system, which will also affect the measurement. The noise problem can be resolved by putting capacitors in parallel to the divider resistors in a similar way as how probe's work, however at higher frequencies this does increase the current drawn by the divider, since the capacitors provide a low impedance path for those frequencies. The final option is to compensate for the current drawn in the microcontroller. This can be done by measuring the voltage, and dividing it by the resistance of the divider, which then gives the current through the divider. From the 3 options, compensating the offset in the microcontroller seems like the most ideal option.

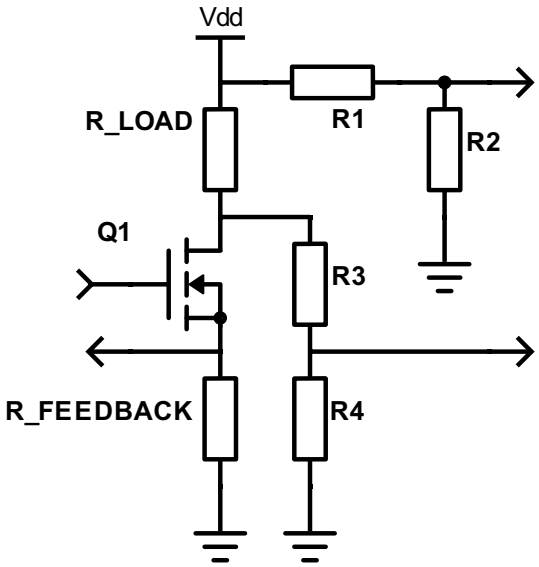

Figure 3.3: Resistive dividers connected to the load resistor

An anti-aliasing filter will be added before the ADC, thus a buffer is required after the resistive divider, so the filter will not load the divider. This buffer will be implemented as a simple voltage follower opamp. The bandwidth of the anti-aliasing filter is limited by the time needed to settle within N bits accuracy, which is given by Equation 3.7 with N being the accuracy in amount of bits.

$$BW = \frac{N \ln(2)}{2\pi t_{settle}} \quad [Hz] \tag{3.7}$$

3.4.2 Crosstalk

The outputs of the 2 dividers have a high impedance, if there are long connections leading from the divider output to the buffer, a reasonably large parasitic capacitance can be present. If an AC signal is sent on one of the divider outputs, it will also appear on the other output due to the parasitic capacitance. There are 2 solutions for this problem, The first is to place the resistive divers very close to the buffer, this will reduce the parasitic capacitance and thus crosstalk between the 2 outputs. The alternative is to put capacitors in parallel with the resistors in the divider, that have the same impedance ratio as the resistors. This will reduce the impedance of the divider at higher frequencies, while not affecting the attenuation. The lower impedance of the divider at higher frequencies can cause a significant offset in the current drawn through the divider. In this design the distance between the divider and the buffer will be kept as short as possible to minimize the low-voltage path and reduce crosstalk. Capacitors will be added only when the previous action is not sufficient.

3.4.3 Resistor Tolerance

Any resistor available will has a tolerance, for surface mount resistors a common tolerance value is 1%. Having this tolerance in the resistive dividers will mean that the dividers can have different attenuation ratios. The maximum value for the tolerance is 0.05% for a 10 bit measurement, and becomes much smaller if the resolution is increased. Especially for higher resolutions, the maximum tolerance is much smaller than any available resistor tolerances. The tolerance of the resistors can be compensated using the microcontroller. However, if the 2 resistive divider outputs would be measured with one differential input analog to digital converter, the voltage on side of the resistor would need to be known already to be able to compensate it. Having 2 separate ADCs to read out each divider separately would allow you to compensate for the tolerance on each divider by multiplying the measured result with the attenuation ratio of the divider. This is much easier to implement since no knowledge of the supply voltage of the system is required for it to work, thus making the system easier to use.

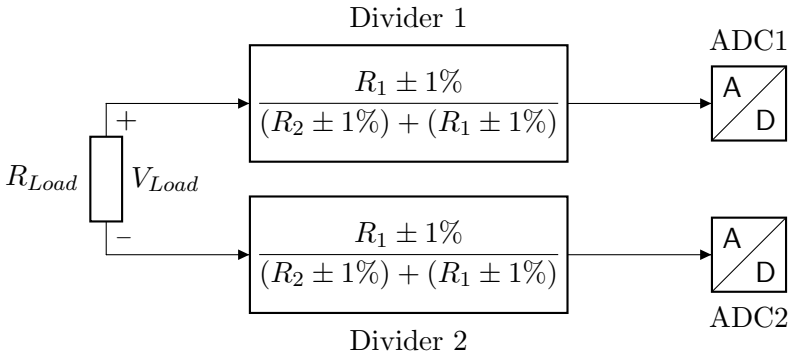

Figure 3.4: Two resistive dividers, with the same intended factor, can vary due to tolerances. Note that the low side of this resistor is not connected to ground

3.4.4 Noise

Choosing high valued resistors has a major downside which is noise. In this subsection the noise voltage added by the resistive divider, the buffer and the anti aliasing filter will be discussed. The expression for the noise power is shown in Equation 3.8. The derivation of this equation can been done using The circuit analysis software SLiCAP. In this equation the Capacitor C1 has been ignored and will be included in the noise bandwidth. It must be noted that for a first order RC filter, the equivalent noise bandwidth is $\frac{\pi}{2}$ times larger than the bandwidth of the RC filter. The schematic used for this analysis in SLiCAP can be seen in section A.1.

$$S_{Vtotal} = S_{Vn} + S_{VR_3} + \frac{(R_1^2 S_{Vcs} + R_1^2 S_{VR_2} + R_2^2 S_{Vn} + (R_1 R_2)^2 S_{In})}{(R_1 + R_2)^2} \qquad \left[\frac{\mathrm{V}^2}{\mathrm{Hz}}\right] \tag{3.8}$$

The noise voltage on the output should be smaller than half of the smallest voltage step the ADC can measure. That way the ADC measurements should not be corrupted by noise. A part of this noise (S_{Vcs}) is produced by the current source in the system, so the maximum noise voltage produced by the measurement setup should be lower than total allowed noise level, to leave some noise room for the current source.

3.5 Current Measurement

3.5.1 Overview

Although a current sensor is not required for the control system to function, monitoring the current through the resistor is useful for validation. The current source in our system is implemented with a 10 Ω feedback resistor [24]. Current delivered to the load also flows through this resistor. Our current sensor measures the voltage across this resistor. The most optimal amplifier for this amplification would be an opamp based voltage amplifier. The connection of the amplifier to the feedback resistor is shown in Figure 3.5. After the amplifier an anti-aliasing filter will be added. Similar to the voltage amplifier, Equation 3.7 sets a minimum requirement to the filter's bandwidth such that the settling of the filter output does not affect the measurement.

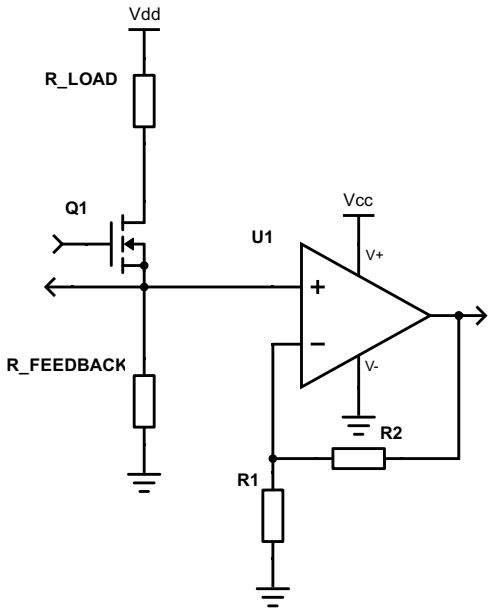

Figure 3.5: connection of the current amplifier to the feedback resistor

3.5.2 Noise

Adding an amplifier to the circuit introduces noise. To prevent noise from influencing the measurements this noise should be smaller than half of the least significant bit of the analog to digital converter. Equation 3.9 is the expression for the noise power of the system. The noise power S_R produced by the resistors can be calculated using Equation 3.8. The expression was derived using SLiCAP. The schematic used in the calculation can be found in section A.2. The capacitor C_1 in the anti aliasing filter has been ignored and will be factored in with the noise

bandwidth in calculation. The equivalent noise bandwidth is defined as the filter bandwidth multiplied by $\frac{\pi}{2}$ for a first order RC low pass filter.

$$S_{Vtotal} = S_{VR3}+S_{VR2} + \frac{(R_1+R_2)^2}{R_1^2}(S_{Vn}+S_{Rshunt}) + \left(\frac{R_2}{R_1}\right)^2 S_{R1}+ \frac{(R_1R_2+R_1R_{shunt}+R_2R_{shunt})^2}{(R_1+R_2)^2} \quad \left[\frac{\mathrm{V}^2}{\mathrm{Hz}}\right] \tag{3.9}$$

The current source which the device is connected to also produces noise (S_{Vcs}), So the readout circuitry should not consume all of the noise budget.

3.6 Pressure Sensor

One of the requirements for the readout circuitry is that it can read out the pressure in the microthruster. To do this two Epcos C32 sensors are placed on the microthruster. The sensor is implemented as a wheatstone bridge, and has a supply voltage range of 1 to 5 V. The sensors operating range is from 0 to 1.6 bar, its sensitivity ranges from 45 to 95 mV/bar with a supply voltage of 5 V and its offset from -50 to 25 mV [25].

3.6.1 Supply Voltage

The supply voltage has a range from 1 to 5 V. Having a larger supply voltage means that the sensors sensitivity will be higher, thus the signal to noise ratio of the pressure sensor output will be higher.

3.6.2 Measurement

The easiest way to measure the 2 outputs of the pressure sensor is by using a differential ADC, since the sensor has differential outputs. The total range of the output signal is from 72 to 152 mV depending on sensitivity of the individual sensor. This signal is rather weak and should be amplified to fit in the ADCs range. This amplification should be limited so that even in the scenario where the the sensitivity and offset are equal to the maximum tolerance, it fits in the ADC range. If the ADC range were to be 5V, which is a common value for ADCs, then a differential gain of 25 times would amplify the signal in such a way that the worst case still fits in the ADC range.

3.6.3 Amplification

Different options are available when it comes to the amplification of the pressure sensor output. The main considerations to take into account are whether to leave the signal as a differential signal, or to convert it to a single ended signal. To convert a differential signal to a single ended signal requires a differential amplifier as shown in Figure 3.6. Since this amplifier does not have an infinite input impedance the output of the pressure sensor needs to be buffered. These buffers will add more noise into the system. The amplifier also has strict requirements on the resistor tolerance of the resistors used, since deviation from ideal values will cause an offset in the signal. The other option is the circuit in Figure 3.7, which has a differential output, thus requiring a differential input ADC. Having a differential input ADC takes away the issue of amplifier offset. The circuit has another benefit in requiring less opamps, which results in less noise on the signal. The combination of less noise and no constraints on resistor tolerance makes the option with a differential output and ADC better. This circuit will also be used in the implementation of the pressure sensor.

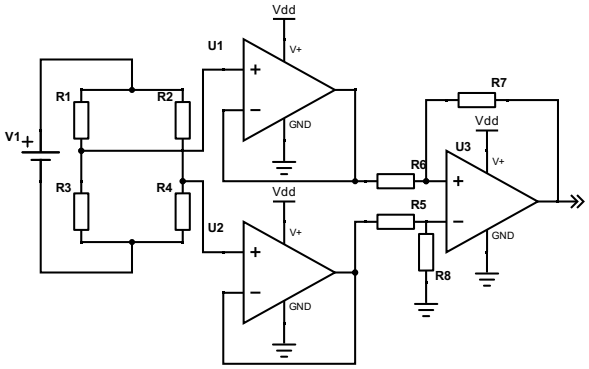

Figure 3.6: Differential amplifier with single ended output

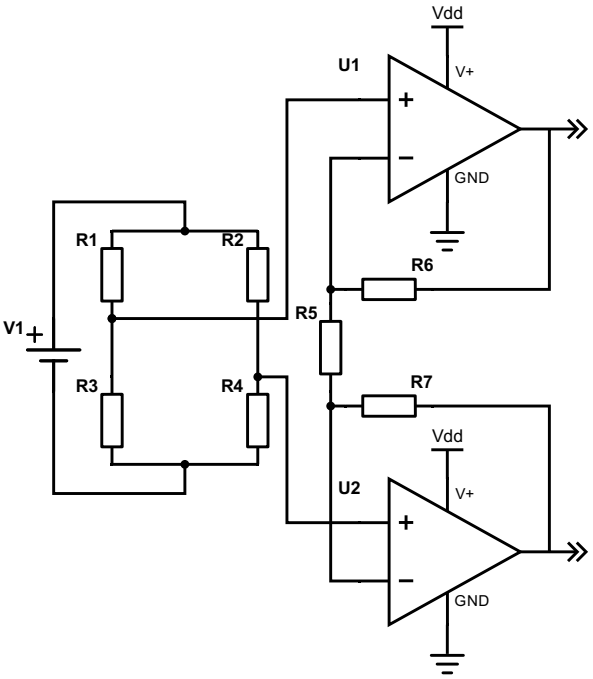

Figure 3.7: Differential amplifier with differential output

3.6.4 Noise

Although there is no requirement for the resolution, and thus no requirement for the noise too, it is preferred to keep the noise produced by the pressure sensor smaller than half of the least significant bit of the ADC. This is done to prevent wasting a part of the ADCs resolution. Equation 3.10. The capacitors C_1 and C_2 in the anti aliasing filter have been ignored and will be factored in with the noise bandwidth in calculation. The noise bandwidth is defined as the filter bandwidth multiplied by $\frac{\pi}{2}$ for a first order RC low pass filter.

$$\begin{aligned} S_{\mathrm{Vtot}} = {} & \mathrm{SR3} + \mathrm{SR4} + \mathrm{SR5} + \mathrm{SR6} + \frac{2\,S_v\,(R_a + 2\,R_b)^2}{{R_a}^2} + \frac{4\,\mathrm{SR2}\,{R_b}^2}{{R_a}^2} \\ & + \frac{\mathrm{SRbridge}\,(R_a + 2\,R_b)^2}{{R_a}^2} + \frac{0.5\,S_i\,(2\,R_a\,R_b + R_a\,R_{\mathrm{bridge}} + 2\,R_b\,R_{\mathrm{bridge}})^2}{{R_a}^2} \end{aligned} \tag{3.10}$$

The equation was derived using SLiCAP, the schematic used do so can be found in section A.3.

3.7 Resistor Temperature coefficient

The resistance value of a resistor depends on the temperature of the resistor. The change of the resistor for a change of 1 °C in temperature is known as the temperature coefficient. This change in resistance should remain small enough to not affect the measurements done by the system in a significant way. Given that the system is meant as an experimental setup which operates in a normal room environment, The system will operate near room temperature. To take some safe margin in the design of this tolerance, the operating temperature range will be from 10 to 30 °C. For the resistor in the anti aliasing filters, the temperature coefficient is not important, since a deviation in resistance value will only change the bandwidth by a very small amount. This can be accounted for by picking a bandwidth slightly higher than what is needed,

so that a tolerance and temperature change wont hurt the systems performance. For the dividers and gain resistors of the amplifiers, the maximum change in resistance due to temperature of the resistance must be smaller than 500 ppm to avoid affecting a 10 bit measurement with a high measurement current. This would lead to a maximum acceptable temperature coefficient of 50 ppm. For higher resolutions the maximum acceptable temperature coefficient would be much lower, however resistors with temperature coefficients much lower than 50ppm will be hard to come by. In those cases some minor temperature drift must be accepted, since it is not something that be easily dealt with.

3.8 Analog To Digital Converter

3.8.1 Resolution

To be able to measure V_{min} as given by Equation 3.4, three variables need to be known. From our requirements, $T_{res} = 1°C$. The available thrusters have $\alpha = 0.0024$ and $R_0 = 680\Omega$. The resulting minimum resolution becomes:

$$N_{min} = \log_2 \left(\frac{V_{max}}{V_{stepsize}} \right) \text{[bits]} \tag{3.11}$$

$$= \log_2 \left(\frac{V_{max}}{I_{meas} \alpha R_0} \right) \tag{3.12}$$

Since the system does need to function with a resistors as small as 100 Ω according to the requirements, some additional resolution is required. Using Equation 3.12 with a measurement current of 70 mA, and a supply voltage of 70V, yields a required resolution of 13 bits. The measurement current of 70 mA has been calculated using Equation 3.5, using the R_0 value of 680 Ω since that is the resistor value for which the system will be optimalised. Since the ability to measure resistances from 100 to 1000 ohm is a trade-of requirement, it should only be implemented if there are no significant disadvantage to it.

3.8.2 Sample Time

The measurement method deemed optimal for this system is the pulse based method. The longer this pulse, the larger the effect on the temperature of the device. Therefore the maximum length of a pulse is limited, and the sample time of the ADC is limited too. The system has been given a sample rate of 1 kHz, and it would be ideal to keep the pulse length shorten than 1% of the sample period to prevent it from affecting the temperature. Thus the maximum sample time an ADC in this system can have is 10 μs. Ideally the sample time of the ADC is shorter than this, if ADC's with shorter sample times for the required resolution are available.

3.8.3 Input Range

The Input range of the ADC is an important parameter, mostly in the application of the pressure sensor. For this application an ADC range of 0 to 5 V is preferred.

3.8.4 Requirements

In Table 3.2 the requirements to the ADC are shown

Requirement	Required Value
Resolution	13 bits
Sample time (without data transfer)	10µs
Input range	0 to 5 V
Input type	Differential and single ended variant (when available)

Table 3.2: Overview of the ADC requirements

3.9 Opamp Requirements

In the readout circuitry some opamps are used, 2 Opamps in a unity gain configuration used as a buffer, and an opamp used to amplify the voltage over the shunt resistor. 2 more opamps will be used in the readout circuit for the pressure sensor. To keep the system simple, it is preferred to use the same model of opamp in all circuits. Since the opamp will be used in a unity gain configuration, It needs to be unity gain stable.

3.9.1 Gain Bandwidth product

Due to the sample rate of the controller of 1 kHz, signals above 500 Hz cannot be measured. To keep the settling time of the opamp fast when a measurement pulse is sent, a much higher Bandwidth is required. This Bandwidth can be calculated using Equation 3.7. In the case of a 16 bit ADC, and a preferred settle time of 5 μs or less, the required bandwidth is 353 kHz. The minimum gain bandwidth product, taking into account the 5x gain of the amplifier amplifying the shunt voltage, is $BW \cdot Gain = 1.765MhHz$. Since the buffer opamp for the voltage measurement is in a unity gain configuration, it's minimum gain bandwidth product requirement will always be lower than that of the amplifier amplifying the shunt voltage. The opamp used for the pressure sensor circuit does not have to deal with fast pulses, so the GBP requirements for the opamps used in this circuit are much lower than the previously mentioned requirements.

3.9.2 Input, Output And Supply

Since The ADCs have a preferred input range of 0 to 5 V, the opamps need to have the same output range. Since a 5 V supply would already be present in the circuit as the reference voltage for the ADC, It would be easy to use this as the supply voltage for the opamp. This does mean that the opamp needs to have a rail-to-rail output, to make use of the full input range of the ADC. Since the opamp will also be used as a buffer in the voltage readout circuit, a rail-to-rail input will also be required.

3.9.3 Input noise

Opamps are not ideal components have produce noise, which is often represented as a voltage and a current noise source on the input. The noise produced by the opamp should be small enough so the measurements by the ADC are not affected, this means that the noise on the opamp output should be smaller than half of the least significant bit of the ADC. The current noise of the opamp will be most noticeable for the buffer amplifier, due to the high impedance connected to its inputs. The noise voltage density at the input of the buffer can be expressed as $V_n + Z_{in} \cdot I_n \ \ [\frac{V}{\sqrt{Hz}}]$, where V_n and I_n are the noise and current voltage densities of the opamp.

The noise voltage produced by the opamp will be most noticeable in the current amplifier, since it provides gain, the noise will also be amplified. The exact calculations on noise will be done when the ADC has been selected and the resolution is known.

3.9.4 Overview

The requirements for the opamp are as follows:

- A minimum Gain-Bandwidth Product of 1.765MHz
- Rail-to-Rail input and output
- Operates on a 5V supply voltage
- Unity gain stable
- Low noise

Chapter 4

Implementation

4.1 Analog to Digital Converter

In chapter 3 the requirements for the ADC's have been determined. The ADC needs at least 13 bits resolution, but more resolution removes the need for a pulse for a part of the voltage range of the ADC. It also opens up the option of increasing the voltage range, which requires more resolution, in case more than 5W needs to be delivered to the load. The minimum sample time was determined to be 10 μs, here faster sampling offers the advantage of having a shorter measurement pulse, which is useful in the case faster sampling is required to stabilise the system.

The ADC that has been selected is the MCP33131. There is a differential and a single ended model available for the ADC, which allows makes it usable for both the pressure sensor and the voltage and current measurements. The MCP33131's main specifications are shown in Table 4.1

Parameter		Value	Unit	Notes
Resolution		16	bits	Differential version has sign bit
Maximum sample rate		1	MSamples/s	
Maximum sample time		300	ns	Without data transfer
Input range	Minimal	0	V	-
	Maximum	V_{ref}	V	$2.5 \leq V_{ref} \leq 5.1$V
Maximum bus speed		100	MHz	SPI Bus

Table 4.1: Main specifications of the selected ADC [26]

4.2 Voltage and Current Measurement

4.2.1 Anti-aliasing filter

The minimum bandwidth of the which is required to keep the settling time of the filter short is given in Equation 3.7 from the previous chapter. Using this equation with a preferred settle time of 10 μs and a resolution of 16 bits gives a minimum bandwidth of 176.5 kHz. To prevent resistor and capacitor tolerance from the filter components reducing the bandwidth below the minimum, 10% headroom should be taken on the minimum bandwidth. This gives a desired bandwidth for the anti aliasing filter of approximately 194.15kHz. This bandwidth is only required for the voltage and current sensors, the pressure sensor is measured continuously so it can have a much lower bandwidth.

Since the selected opamp does not drive capacitors above 100pF in a unity gain configuration, the capacitance should be kept relatively low. The values selected to comply with this

and the desired bandwidth are a 10 $k\Omega$ resistor, and a 82 pF capacitor. An RC filter using those components has a cutoff frequency of 194.1 kHz, which is extremely close the the desired bandwidth of 194.15 kHz.

The exact same bandwidth requirements apply to the current measurement, so the same anti aliasing filter will be used in the current measurement circuit.

4.2.2 Resistive Divider Values

The voltage measurement circuit needs to have a divider to attenuate the voltage, there is a trade-off to make between noise and offset for this circuit. Having a 16 bit resolution on the ADC means that the least significant bit has a value of 76.3 µV for a Vref of 5 V. Thus the noise on the half this value, which equals 38.15 μV. Not all of this noise room should be used by the divider, since the current source and the opamp also add noise to the system. For this division, values of 680 $k\Omega$ and 47 $k\Omega$ have been selected. This reduces the leakage current to 100 μA when 70 volt is connected to the input. This current flowing through the load resistor, but not through the shunt resistor causes an offset voltage of 70 mV for a 700 Ω resistor, which is too large to ignore. The compensation of this offset will be discussed in a dedicated section. The noise generated by the resistors on the divider output is small enough to comply with the requirement. The calculation total system noise will be covered in a dedicated subsection.

4.2.3 Current Amplifier Gain Resistors

In the selection of the gain resistors there are 2 major factors that should be considered: noise and current draw. Most opamps cannot deliver large currents, so the resistors should have values high enough to keep the current low. The resistors should also not be too large, since they will introduce a lot of noise in that scenario. The values that have been selected for the amplifier shown in Figure 3.5 are 4.7 kΩ for R_2 and 1.2 kΩ for R_1. This gives a gain of 4.9, which is close to the desired value of 5. The maximum current draw on a 5 V supply voltage is 0.85 mA, which is a current most opamps can handle. The noise generated by the circuit will be covered in a separate subsection.

4.2.4 Opamp selection

The opamp selected the meet the requirements presented in the previous chapter is the MCP6292. A short summary of its specifications:

- 10MHz Gain-Bandwidth Project
- Rail-to-Rail inputs and outputs
- 100pF Capacative load
- 8.7 $\frac{nV}{\sqrt{Hz}}$ noise voltage, 3 $\frac{fA}{\sqrt{Hz}}$ noise current
- Supply voltage from 2.4V to 6.0V

4.2.5 Voltage Measurement Noise

To calculate the noise on the ADC input, Equation 3.8 will be used, The noise produced by the current source will temporarily be ignored. Table 4.2 shows the parameters used in the noise calculation.

Parameter name	Value	Unit
Signal Bandwidth B_s	194.1	kHz
R_1	47	kΩ
R_2	680	kΩ
R_3	10	kΩ
V_n	8.7×10^{-9}	$V/\sqrt{Hz}$
I_n	3×10^{-15}	$A/\sqrt{Hz}$
T	293.15	K

Table 4.2: Parameters used in the noise calculation

Filling in the parameters in the equation results in a noise power $2.89 \times 10^{-10}\,V^2$, and a noise voltage of 17.0µV. This leaves $1.15 \times 10^{-9}\,V^2$ of noise power available for current source, or a noise voltage of 34.0µV on the ADC input. Since the noise voltage from the current source is divided 15.47 times the acceptable noise voltage on the input of the divider is 525.6µV.

4.2.6 Current Measurement Noise

To calculate the noise on the ADC input, Equation 3.9 will be used, The noise produced by the current source on the shunt resistor will temporarily be ignored. Table 4.3 shows the parameters used in the noise calculation.

Parameter name	Value	Unit
Signal Bandwidth B_s	194.1	kHz
R_1	1.2	kΩ
R_2	4.7	kΩ
R_3	10	kΩ
V_n	8.7×10^{-9}	$V/\sqrt{Hz}$
I_n	3×10^{-15}	$A/\sqrt{Hz}$
T	293.15	K

Table 4.3: Parameters used in the noise calculation

Filling in the parameters in the equation results in a noise power $4.6 \times 10^{-10}\,V^2$, and a noise voltage of 21.5µV. This leaves $1.0 \times 10^{-9}\,V^2$ noise power available for current source, or a noise voltage of 31.6µV on the ADC input. Since the noise voltage from the current source amplified 4.9 times the acceptable noise voltage on the input of the divider is 6.44µV.

4.3 Pressure measurement

4.3.1 Gain Resistors

For the pressure measurement a gain of 25 times has been selected in the previous chapter. To realise this gain the differential amplifier from Figure 3.7 is implemented. The gain of such an amplifier is given by $1 + \frac{R_6+R_7}{R_5}$. Given the required gain of 25, R_6 and R_7 have been given values of 12 kΩ and R_5 a value of 1 kΩ.

4.3.2 Anti-aliasing filter

The pressure Sensor will be sampled at 1 kSamples/s, meaning that the highest frequency that can be measured will be 500 Hz. The filter is implemented as a first order RC filter,

because of their simplicity and size. The anti aliasing filter for the pressure sensor will be set to approximately 5kHz, such that the filter will not affect the response in the frequency band of interest. In this filter a $390\Omega k$ and a 82pF capacitor will be used. This gives a cutoff frequency of 4977 Hz.

4.3.3 Pressure Measurement Noise

Although there are no requirements for the pressure sensor's resolution, the noise on the input should preferably be low enough to use the 15 bits resolution of the available differential ADC. The 4 Wheatstone bridge resistors from the pressure sensor have been represented as a single bridge resistance R_{bridge} in this noise calculation.

Parameter name	Value	Unit
Signal Bandwidth B_s	4977	Hz
R_{Bridge}	3.3	kΩ
R_5	1	kΩ
R_6	12	kΩ
R_7	12	kΩ
V_n	8.7×10^{-9}	$V/\sqrt{Hz}$
I_n	3×10^{-15}	$A/\sqrt{Hz}$
T	293.15	K

Table 4.4: Parameters used in the noise calculation

This gives a noise power on the ADC input of $1.18 \times 10^{-9}\,V^2$, which translates to a noise voltage of 34.4µV. This value is below the maximum noise threshold of 76.3µV, which follows from a voltage range of 5V and a resolution of 15 bits.

4.4 Offset Compensation

Due to resistor tolerances, and the current drawn through the resistive divider, some offsets are created in the system. Those offsets need to be compensated, which is easily done in the micro-controller that controls the thruster. For some of the different circuits the compensation method will be discussed.

Voltage Attenuation Offset The resistors which are used in the divider have some tolerance, thus the attenuation will not be exactly the calculated value. To compensate for this, the exact attenuation needs to be measured. This measured value is then used in the micro-controller to calculate the actual voltage over the load.

Current Gain Offset The resistor used in the amplifier for the shunt resistor also has a tolerance, this will cause the gain to have some tolerance too. This can be compensated by measuring the exact gain, which can then be used in the microcontroller to calculate the real current.

Current draw by the resistive divider The resistive dividers have a finite impedance and thus draw a current. This current which is drawn will flow through the load, but not to through the shunt resistor. This added load current is large enough to affect the measurements significantly. The current through the divider is proportional to the voltage over the divider, which is measured by an ADC. This allows the additional current to be calculated and added to the current measured through the shunt.

Reference Voltage The ADCs have a reference voltage which defines their input range. This voltage is not exactly 5 volts, this causes a significant offset. It can be compensated by measuring the exact reference voltage, and by adding this voltage as a factor in the micro-controller.

Pressure Sensor The pressure sensor circuit has 2 main causes for offset. The first offset is the gain of the differential amplifier, which is not exact. The second is the offset from the pressure sensor itself, which consists of a tolerance in sensitivity, and a fixed offset. To compensate for this the sensitivity offset and the fixed offset of the total system should be measured, and then added to the micro-controller as a factor and a fixed value.

4.5 Prototype Circuits

Before a pcb was designed the circuits were implemented on a prototype board. The circuits were built as the same way as described in chapter 3 and 4 except for a small difference. This difference is described in section 4.6. All measurements done in results will be done with this prototype circuit. Images of the prototype circuits can be found in Appendix B. The ADCs and opamps used in the prototype circuits have all been equipped with bypass capacitors with values as they are specified in the datasheets of the components.

4.6 ADCs

In the prototype circuits for the current and voltage measurements there is a small difference with the ADCs. Instead of single ended ADCs, differential ADCs were used. This means that the resolution of those systems is 15 bits instead of 16. The voltage measurement has also been implemented with only 1 ADC, connecting the outputs of the dividers to the differential input. To compensate for resistor tolerance a different compensation scheme has been used, which relies on knowing the supply voltage connected to the high side of the heater resistor. It should operate virtually the same compared to how the system was originally designed.

4.7 PCB Design

4.7.1 Schematic

All schematics from our subgroup and the current source group were merged into one big project. This schematic differs in a few places from our prototype circuits:

1. Reverse polarity protection on the power supply inputs
2. Fused supply inputs
3. The DAC uses a mcp1501 voltage reference for VREF
4. Pressure sensors are powered by the microcontroller
5. The DAC, ADC and current source circuits are isolated from the microcontroller
6. The resistive divider for the voltage measurement contains a trimmer resistor in order to tune the attenuation

The full schematic can be found in section D.1.

4.7.2 Connectors

The PCB is designed to as an add-on board for the NUCLEO STM32F767 microcontroller board. The PCB is about the same size as the NUCLEO, and connects directly on top of the 144 pins. Additionally, two pairs of banana plugs where added: one for the high-voltage power supply which powers the current source, and a low-voltage supply input for our ICs.
The thruster boards at our disposal use standard 2.54mm spaced pins as connectors. We opted to put female versions of these headers on our PCB for power supply and voltage measurement. This prevents somebody accidentally touching to pins while high voltage is present. Lastly, each of the two pressure sensors has its own 2.54mm header which exposes 5V and GND for the wheatstone bridge, and two connections for the differential measurement.

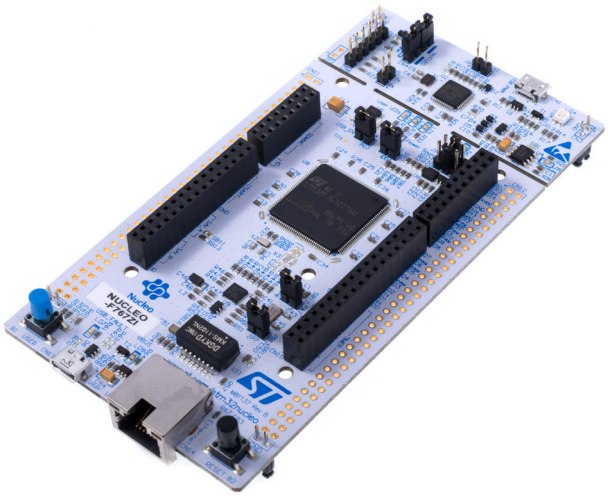

Figure 4.1: An STM32 NUCLEO-F767ZI board

Chapter 5

Results

5.1 Verfication Method

To confirm whether the system can measure a difference of 1°C the accuracy of the voltage and current measurement has to be verified. For the system to measure this temperature difference, an accurate resolution of at least 13 bits was required, thus noise should be small enough to not affect the measurement at 13 bits.
To test the noise levels in our system a low-noise voltage source was applied to the input of every subsystem. To realize a voltage source with a lower noise level than the system itself, a resistive divider was build with a large capacitor at the output. This capacitor was chosen to limit the bandwidth below the 100 mHz. In all cases, the source was connected to the input of the specific measurement circuit. A microcontroller continuously sampled the ADC. The resulting values were collected and are presented in the following sections. Note that the graphs contain the 16-bit binary value from the ADC translated into a decimal. All samples were taken with $t_{sample} = 1\mu s$. The frequency values corresponding to the histograms can be found in Appendix C.
To verify whether amplifiers and the dividers functioned properly, sine waves with known amplitudes and frequencies 1 and 100 Hz are put on the input. The output is then measured using a microcontroller. If the amplifiers, buffers, or dividers work a signal with the proper amplitude should be measured.

5.2 Voltage Measurement Circuit

5.2.1 Amplitude Measurements

In this measurement a sine wave with a measured voltage from 50 mV to 10 V is connected to the input of one of the dividers, the other input has been connected to ground. The measurement results are shown in Figure 5.4. From this figure it can be seen that the measured value has an amplitude of approximately 0.63 V. Given the max input voltage of 10 V, the attenuation is 15.87 times. This is close to the value which the divider was originally designed for. It should be noted that at the bottom some clipping occurs, this clipping is caused by the buffer opamps, since its output need to stay away from the supply rails by a few mV.

5.2.2 Measurement Noise

In this measurement no compensation schemes were used, as the only purpose of the measurement was to confirm that noise did not obstruct using all 15 bits of the ADC. In figure 5.1 results from two different voltages are shown. In figure 5.1a About 65% of samples resulted into one binary value. At the other voltage, the samples spread across two values: 93% of our readings fit in of these two values.

5.3 Current Measurement Circuit

5.3.1 Amplitude Measurements

Figure 5.5 shows the output of the current sensor with a sine wave on the input with a voltage from 50 mV to 950 mV. The figure shows measured values of approximately 0.25 V to 4.6 V. This results in a gain of 4.83, close to the designed value of 4.917 .

5.3.2 Measurement Noise

Under normal operating conditions, the current measurement circuit would measure the voltage across the $10\,\Omega$ feedback resistor. In this test, the voltage from the voltage reference was measured instead. Three measurements at different voltage levels were performed. The results are shown in Figure 5.2. The measurements at $V_{in} = 0.486V$ and $V_{in} = 0.974V$ are 100% precise: all values fit in one code. At $V_{in} = 47\text{mV}$, the measurements are less precise.

5.4 Pressure Measurement Circuit

5.4.1 Amplitude Measurements

Figure 5.6 shows the output of the pressure sensor with 2.5 V on one input, and a sine wave with a voltage from 2.45 to 2.55 V. The offset visible in the measurement is caused by the fact that 2 different voltage sources were used on the 2 inputs, which introduces an offset on the input. The peak-to-peak value of the measured signal is approximately 2.5 V. Given the 100 mV peak-to-peak value of the sine wave on the input, the gain of the system is determined to be 25, which is close to the gain of 25 which the system was designed for.

5.4.2 Measurement Noise

The pressure sensor circuit was tested with a voltage of 121mV at the input, and then tested again with the polarity reversed. The results are visible in figures 5.3a and 5.3b. When reversing the polarity, more noise is present while the same offset is applied. We have no explanation for this phenomenon. It is possible that the ADC might function slightly different with negative differential inputs. Next, the circuit was tested with the pressure sensor at the input, while the pressure was set to a fixed value. This is visible in Figure 5.3c.

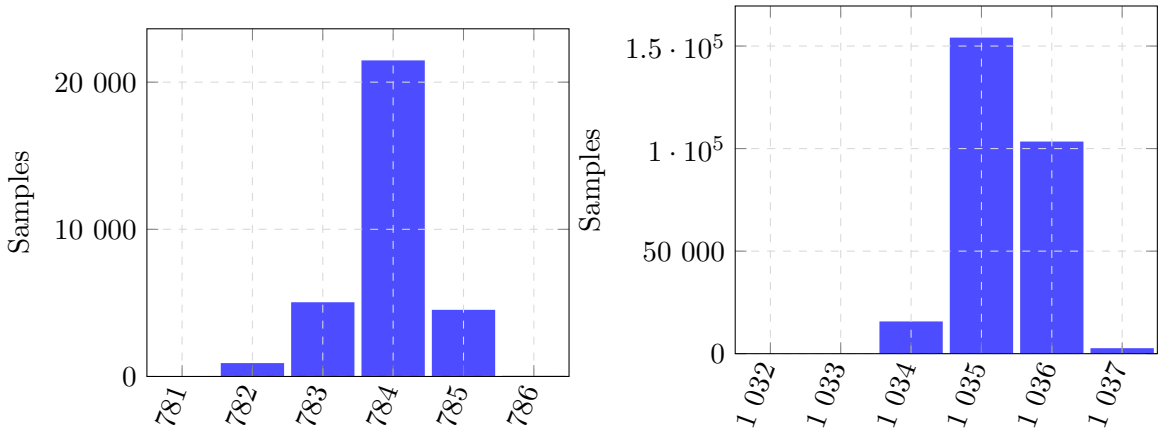

(a) $V_{in} = 1.895V$, $N_{samples} = 32000$ (b) $V_{in} = 2.515V$, $N_{samples} = 276000$

Figure 5.1: Code histograms for voltage measurement

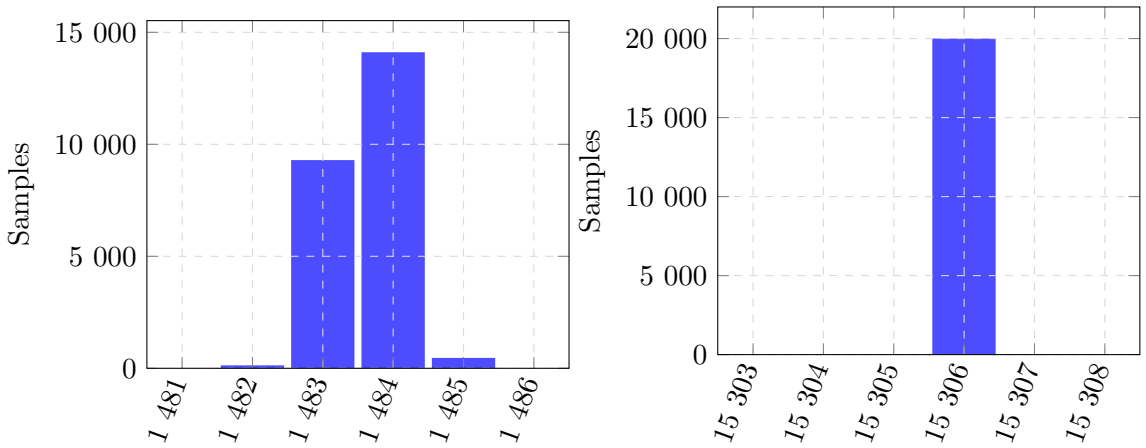

(a) $V_{in} = 0.047V$, $N_{samples} = 24000$ (b) $V_{in} = 0.486V$, $N_{samples} = 20000$

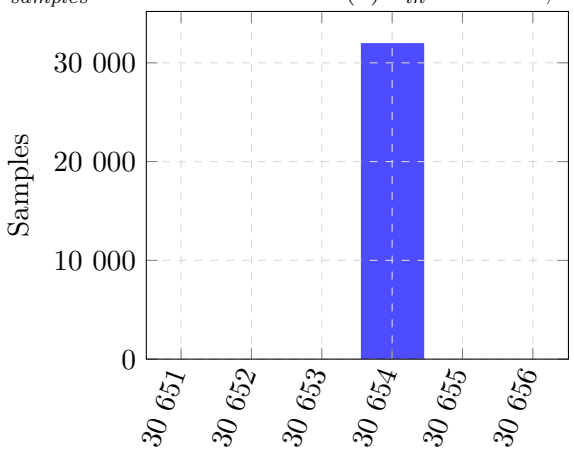

(c) $V_{in} = 0.974V$, $N_{samples} = 32000$

Figure 5.2: Code histograms for the current sensor circuit with different input voltages

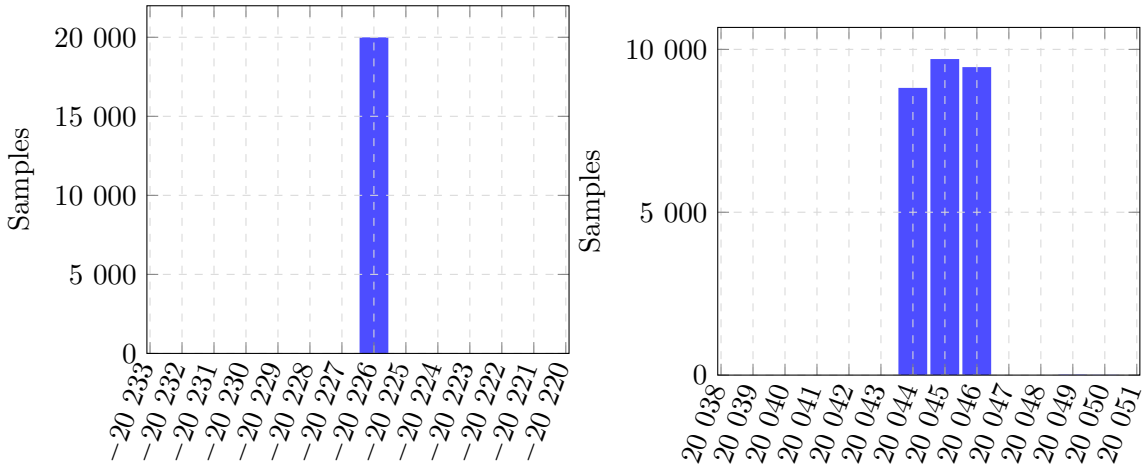

(a) $V_{in} = 0.121\text{V}$, $N_{samples} = 20000$ (b) $V_{in} = -0.121\text{V}$,$N_{samples} = 28000$

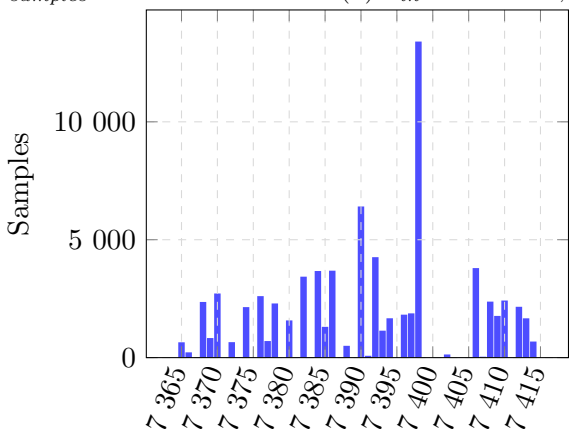

(c) Pressure sensor attached, $N_{samples} = 78982$

Figure 5.3: Code histograms for the pressure sensor measurement

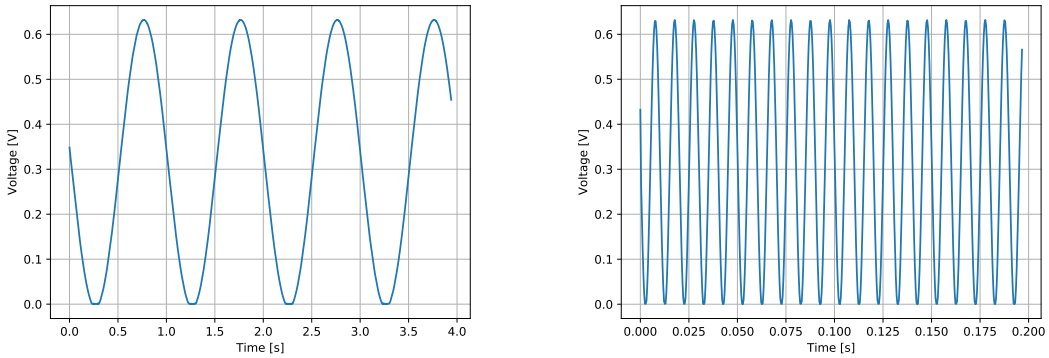

(a) $f = 1\text{Hz}$, $V_{min} = 0.050\text{V}$, $V_{max} = 10\text{V}$ (b) $f = 100\text{Hz}$, $V_{min} = 0.050\text{V}$, $V_{max} = 10\text{V}$

Figure 5.4: Voltage sensor circuit with a sine wave at the input with frequency f

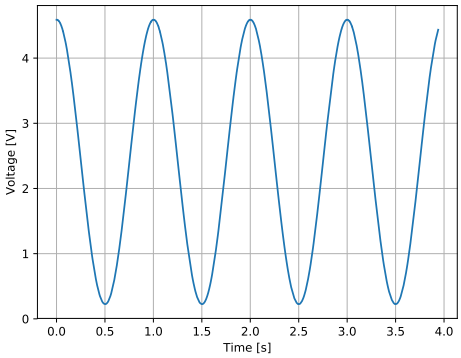

(a) $f = 1\text{Hz}$, $V_{min} = 0.050\text{V}$, $V_{max} = 950\text{mV}$

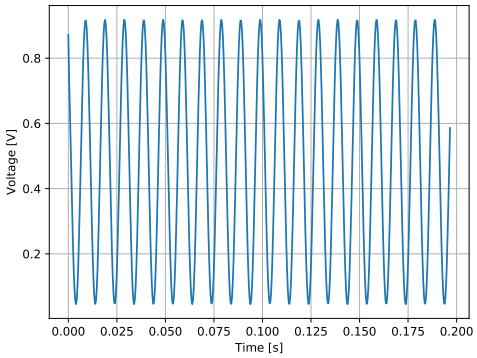

(b) $f = 100\text{Hz}$, $V_{min} = 0.050\text{V}$, $V_{max} = 950\text{mV}$

Figure 5.5: Voltage sensor circuit with a sine wave at the input with frequency f

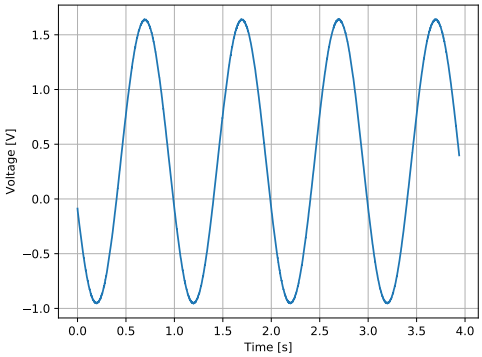

(a) $f = 1\text{Hz}$, $V_{min} = 2.450\text{V}$, $V_{max} = 2.550\text{V}$

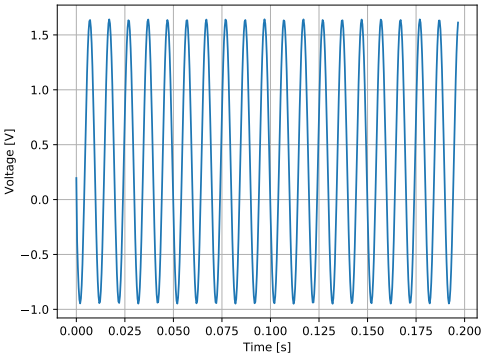

(b) $f = 100\text{Hz}$, $V_{min} = 2.450\text{V}$, $V_{max} = 2.550\text{V}$

Figure 5.6: Pressue sensor circuit with a sine wave at the input with frequency f

Chapter 6

Conclusion

The main target of the project was to control the temperature of a microthrusters heater and to be able to extract the measurement data to a computer. Multiple methods to measure the temperature and pressure have been considered, the method based on time-main separation has been implemented. In this implementation resolution, noise and various causes for offset have been discussed. From the program of requirements, the accuracy of the temperature measurement has been verified by measuring whether the ADC can actually measure with a resolution equal or higher to the 13 bits minimum resolution which is required for 1 °C accuracy. In this implementation, a resolution of 15 bits is provided, which allows for more accuracy, or for measurements with a lower measurement current. The requirement that states that the resistor must be used as both heater and a sensor has been met by design. The same applies the the requirement which states that a 4 probe measurement is required. The requirement of the temperature not being affected by the measurement could not be verified, since this verification required the system integration to be finished, which is not the case. Given the time constant of 20 seconds[27] and the minimum measurement pulse length of 10 µs, we expect the temperature of the heater not to be affected significantly during measurement. The requirement of being able to readout 2 EPCOS pressure sensors has also been fulfilled. Although no requirements to the resolution of this measurement were given, the final implementation has a 15 bit resolution, which should be more than sufficient to provide accurate measurements. The requirement of the system being able to be connected to a different load has been met. The system has not been optimized for resistors smaller than 700 Ω, however due to the additional resolution implemented in the design, it is possible to measure the temperature with sufficient accuracy for resistors down to 100 Ω. Due to time constraints the measurement and control of more than one microthruster could not be implemented. To conclude, all requirements in the program of requirements that apply to the readout of the temperature have been met, except for the ability to read out multiple thrusters, and the measurements not affecting the temperature of the heater since this has not been verified yet. Since these requirements have been met, the readout system in its current state is ready to be used by the control system.

Chapter 7

Recommendations

Although the system is functional, there are still some requirements that have not been met completely, and more data of the performance of complete system have to be gathered. Before the system would be usable on a larger scale, some work has to be done on the system:

- The effect of the measurement pulses on the system temperature should be measured to verify whether the effects are actually negligible.
- More measurements of the complete system should be produced, so that the functionality of the system as a whole can be confirmed.
- The system could be redesigned in such a way that it can control and acquire data from multiple microthrusters
- A more compact PCB could be designed that has the micro-controller integrated on the PCB itself
- Measurements can be done to verify whether stabilizing the temperature with a control system also stabilises the thrust of the microthuster.

Chapter 8

References

[1] J. Bouwmeester and J. Guo, "Survey of worldwide pico- and nanosatellite missions, distributions and subsystem technology," *Acta Astronautica*, vol. 67, no. 7, pp. 854–862, 2010, ISSN: 0094-5765. DOI: https://doi.org/10.1016/j.actaastro.2010.06.004. [Online]. Available: http://www.sciencedirect.com/science/article/pii/S0094576510001955.

[2] M. A. Silva, M. Shan, A. Cervone, and E. Gill, "Fuzzy control allocation of microthrusters for space debris removal using cubesats," *Engineering Applications of Artificial Intelligence*, vol. 81, pp. 145–156, 2019, ISSN: 0952-1976. DOI: https://doi.org/10.1016/j.engappai.2019.02.008. [Online]. Available: http://www.sciencedirect.com/science/article/pii/S0952197619300314.

[3] E. Gill, P. Sundaramoorthy, J. Bouwmeester, B. Zandbergen, and R. Reinhard, "Formation flying within a constellation of nano-satellites: The qb50 mission," *Acta Astronautica*, vol. 82, no. 1, pp. 110–117, 2013, 6th International Workshop on Satellite Constellation and Formation Flying, ISSN: 0094-5765. DOI: https://doi.org/10.1016/j.actaastro.2012.04.029. [Online]. Available: http://www.sciencedirect.com/science/article/pii/S0094576512001440.

[4] L. Felicetti and F. Santoni, "Nanosatellite swarm missions in low earth orbit using laser propulsion," *Aerospace Science and Technology*, vol. 27, no. 1, pp. 179–187, 2013, ISSN: 1270-9638. DOI: https://doi.org/10.1016/j.ast.2012.08.005. [Online]. Available: http://www.sciencedirect.com/science/article/pii/S1270963812001253.

[5] "Nasa technology roadmaps," *TA 2: In-Space Propulsion Technologies*, 2015.

[6] E. Kulu, *Nanosats database*. [Online]. Available: www.nanosats.eu.

[7] K. Lemmer, "Propulsion for cubesats," *Acta Astronautica*, vol. 134, pp. 231–243, 2017, ISSN: 0094-5765. DOI: https://doi.org/10.1016/j.actaastro.2017.01.048. [Online]. Available: http://www.sciencedirect.com/science/article/pii/S0094576516308840.

[8] M. A. Silva, D. C. Guerrieri, A. Cervone, and E. Gill, "A review of mems micropropulsion technologies for cubesats and pocketqubes," *Acta Astronautica*, vol. 143, pp. 234–243, 2018, ISSN: 0094-5765. DOI: https://doi.org/10.1016/j.actaastro.2017.11.049. [Online]. Available: http://www.sciencedirect.com/science/article/pii/S0094576517304290.

[9] M. A. Silva, D. C. Guerrieri, H. van Zeijl, A. Cervone, and E. Gill, "Vaporizing liquid microthrusters with integrated heaters and temperature measurement," *Sensors and Actuators A: Physical*, vol. 265, pp. 261–274, 2017, ISSN: 0924-4247. DOI: https://doi.org/10.1016/j.sna.2017.07.032. [Online]. Available: http://www.sciencedirect.com/science/article/pii/S0924424717306490.

[10] D. Selva and D. Krejci, "A survey and assessment of the capabilities of cubesats for earth observation," *Acta Astronautica*, vol. 74, pp. 50–68, 2012, ISSN: 0094-5765. DOI: https://doi.org/10.1016/j.actaastro.2011.12.014. [Online]. Available: http://www.sciencedirect.com/science/article/pii/S0094576511003742.

[11] A. Cervone, B. Zandbergen, J. Bouwmester, and J. Guo, "Micro-propulsion research; challenges towards future nano-satellite projects," *Leonardo Times*, 2013. [Online]. Available: http://resolver.tudelft.nl/uuid:c1757611-8f73-4061-a573-d748aaa36b23.

[12] A. Tummala and A. Dutta, "An overview of cube-satellite propulsion technologies and trends," *Aerospace*, vol. 4, Dec. 2017. DOI: 10.3390/aerospace4040058.

[13] A. Cervone, B. Zandbergen, D. C. Guerrieri, M. De Athayde Costa e Silva, I. Krusharev, and H. van Zeijl, "Green micro-resistojet research at delft university of technology: New options for cubesat propulsion," *CEAS Space Journal*, vol. 9, no. 1, pp. 111–125, Mar. 2017, ISSN: 1868-2510. DOI: 10.1007/s12567-016-0135-3. [Online]. Available: https://doi.org/10.1007/s12567-016-0135-3.

[14] D. J. Laser and J. G. Santiago, "A review of micropumps," *Journal of Micromechanics and Microengineering*, vol. 14, no. 6, R35–R64, Apr. 2004. DOI: 10.1088/0960-1317/14/6/r01. [Online]. Available: https://doi.org/10.1088%2F0960-1317%2F14%2F6%2Fr01.

[15] N.-T. Nguyen, X. Huang, and T. K. Chuan, "Mems-micropumps: A review," *Journal of fluids Engineering*, vol. 124, no. 2, pp. 384–392, 2002.

[16] J. Tsai and L. Lin, "Transient thermal bubble formation on polysilicon micro-resisters," *Journal of Heat Transfer*, vol. 124, pp. 375–382, 2002. DOI: 10.1115/1.1445136.

[17] K. T. Wen-Jei Yang, "Overview of boiling on microstructures - macro bubbles from micro heaters," *Microscale Thermophysical Engineering*, vol. 4, no. 1, pp. 7–24, 2000. DOI: 10.1080/108939500199600. eprint: https://doi.org/10.1080/108939500199600. [Online]. Available: https://doi.org/10.1080/108939500199600.

[18] N. Miyakawa, W. Legner, T. Ziemann, D. Telitschkin, H.-J. Fecht, and A. Friedberger, "Mems-based microthruster with integrated platinum thin film resistance temperature detector (rtd), heater meander and thermal insulation for operation up to 1,000c," *Microsystem Technologies*, vol. 18, no. 7-8, pp. 1077–1087, 2012. DOI: 10.1007/s00542-012-1441-0. [Online]. Available: https://link.springer.com/content/pdf/10.1007%2Fs00542-012-1441-0.pdf.

[19] J. O. Dennis, A. A. Rabih, M. H. M. Khir, A. Y. Ahmed, M. G. Ahmed, and M. U. Mian, "Characterization of embedded microheater of a cmos–mems gravimetric sensor device," *Microelectronics Journal*, vol. 55, pp. 179–188, 2016, ISSN: 0026-2692. DOI: https://doi.org/10.1016/j.mejo.2016.07.005. [Online]. Available: http://www.sciencedirect.com/science/article/pii/S002626921630266X.

[20] J. Han and M. Meyyappan, "A built in temperature sensor in a integrated microheater," *IEEE Sensors*, vol. 16, no. 14, 2016. [Online]. Available: https://ieeexplore.ieee.org/document/7480357.

[21] T. D. MacGee, *Principles and methods of temperature measurement*. New York: John Wiley & Sons, 1988.

[22] P. R. N. Childs, J. R. Greenwood, and C. A. Long, "Review of temperature measurement," *Review of Scientific Instruments*, vol. 71, no. 8, pp. 2959–2978, 2000. DOI: 10.1063/1.1305516. eprint: https://doi.org/10.1063/1.1305516. [Online]. Available: https://doi.org/10.1063/1.1305516.

[23] S. D. Stearns, H. Cai, J. A. Koehn, M. Brisbin, C. Cowles, C. Bishop, S. Puente, and D. Ashworth, "A direct resistively heated gas chromatography column with heating and sensing on the same nickel element," *Journal of Chromatography A*, vol. 1217, no. 27, pp. 4629–4638, 2010, ISSN: 0021-9673. DOI: https://doi.org/10.1016/j.chroma.2010.04.050. [Online]. Available: http://www.sciencedirect.com/science/article/pii/S0021967310005364.

[24] M. Mrahorović and K. Lam, "Design and implementation of a power supply for mems vaporizing liquid microthrusters."

[25] *Pressure sensors aer xx.xx c32/2 f00 g08 n*, EPCOS, 2017. [Online]. Available: https://www.tdk-electronics.tdk.com/inf/57/ds/c32_gauge.pdf.

[26] *1 msps/500 ksps 16/14/12-bit single-ended input sar adc*, DS20006122A, Microchip Technology, 2018.

[27] G. Breysens and M. Rebers, "Control and data-acquisition of a heater/temperature sensor."

.

Appendix A

Noise Calculations

A.1 Voltage Measurement

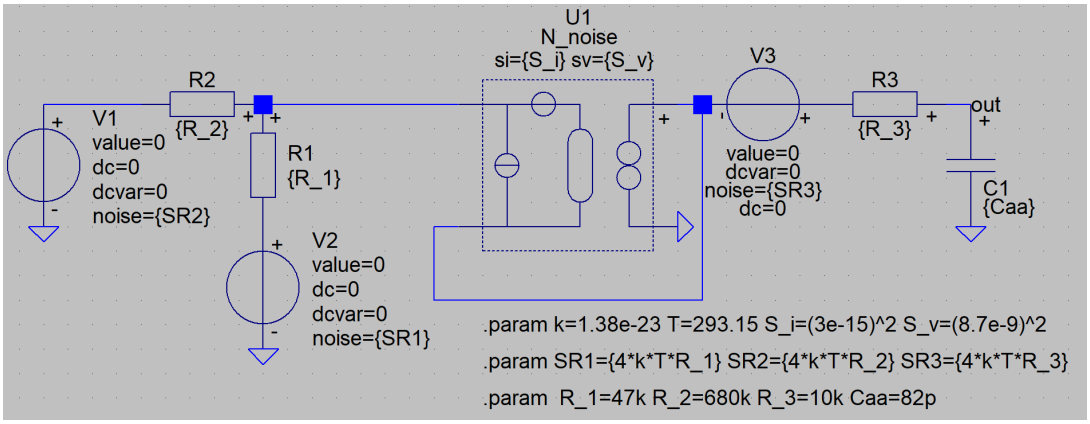

Figure A.1: Schematic used to calculate the voltage sensor noise in SLiCAP

A.2 Current Measurement

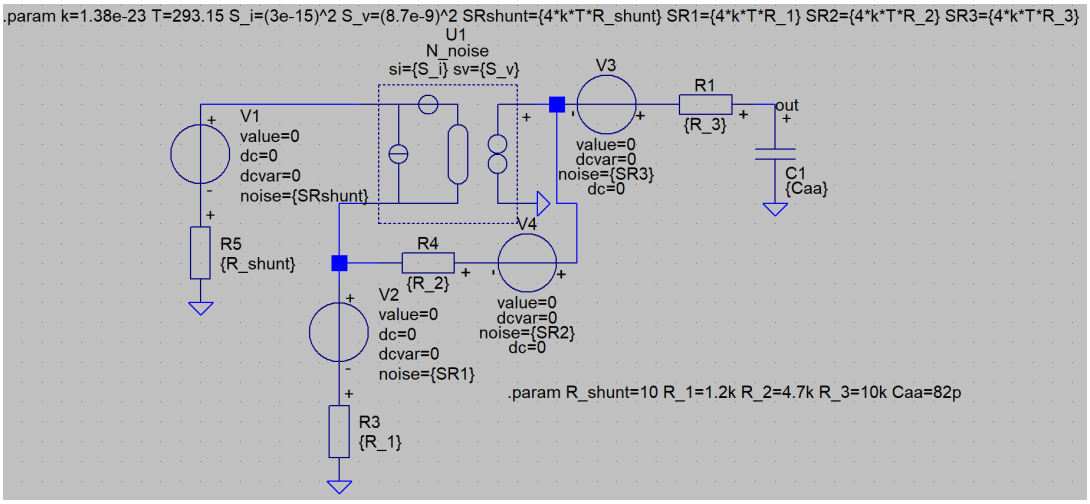

Figure A.2: Schematic used to calculate the current sensor noise in SLiCAP

A.3 Pressure Measurement

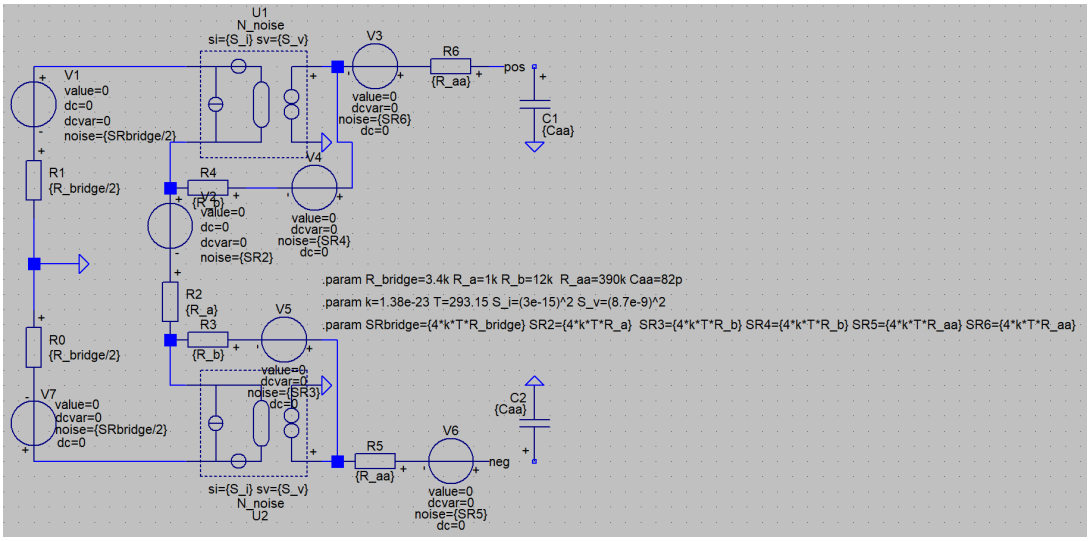

Figure A.3: Schematic used to calculate the Pressure sensor noise in SLiCAP

Appendix B

Prototype Circuit

B.1 Voltage And Current Readout Circuit

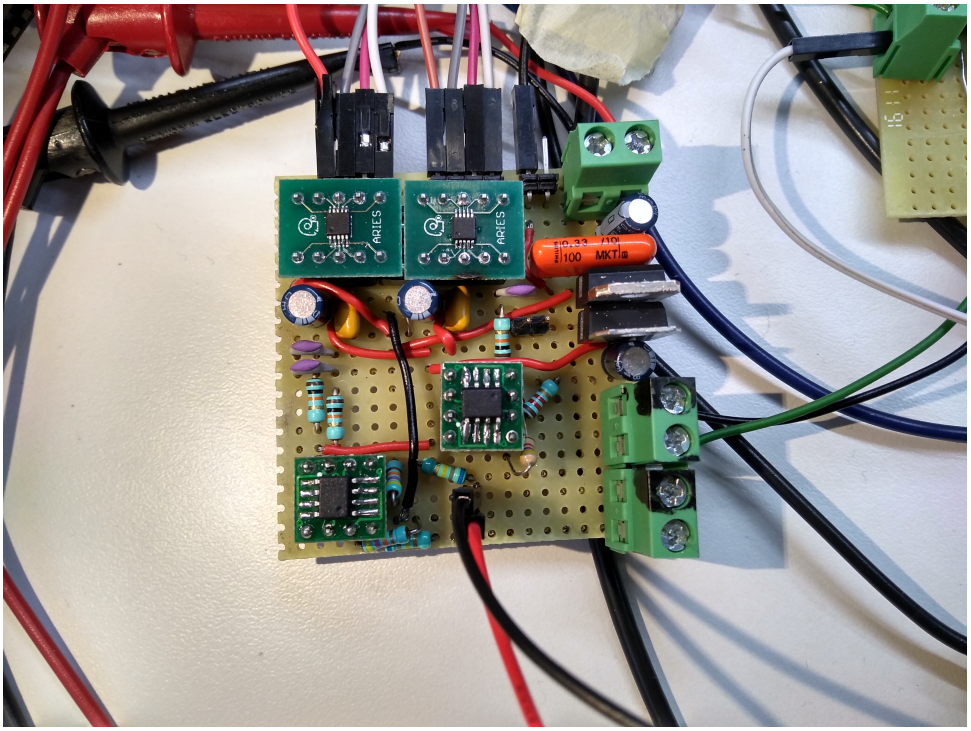

Figure B.1: Prototype circuit for the voltage and current measurement

B.2 Pressure Readout Circuit

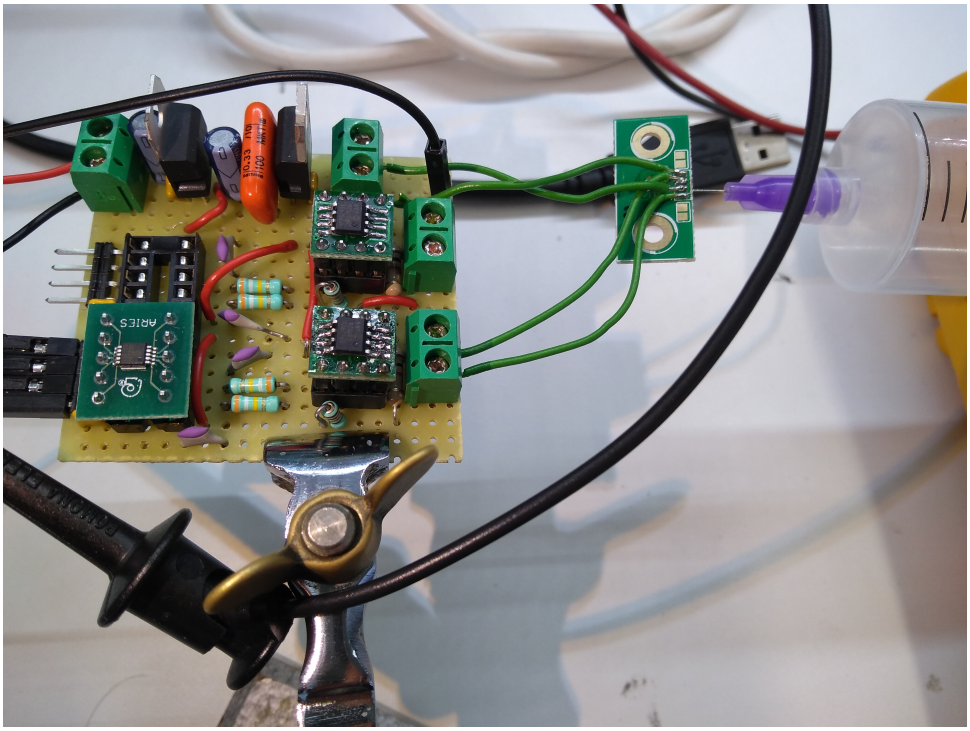

Figure B.2: Prototype circuit for the pressure measurement

Appendix C

Raw Noise Measurements

C.1 Voltage Sensor

Code	Count
1033	59
1034	15712
1035	154117
1036	103434
1037	2677
1038	1

Table C.1: Sampled words from the voltage measurement ADC with $V_{in} = 2.515$V

	Count
782	908
783	5043
784	21478
785	4528
786	43

Table C.2: Sampled words from the voltage measurement ADC with $V_{in} = 1.895$V

C.2 Current Sensor

	Count
1482	131
1483	9295
1484	14110
1485	464

Table C.3: Sampled words from the current measurement ADC with $V_{in} = 47$mV

	Count
15306	20000

Table C.4: Sampled words from the current measurement ADC with $V_{in} = 486\text{mV}$

	Count
30654	32000

Table C.5: Sampled words from the current measurement ADC with $V_{in} = 974\text{mV}$

C.3 Pressure Sensor

	Count
-20230	5
-20226	19994
-19678	1

Table C.6: Sampled words from the pressure measurement ADC with $V_{in} = 121\text{mV}$

	Count
20038	1
20044	8817
20045	9703
20046	9455
20049	15
20050	9

Table C.7: Sampled words from the pressure measurement ADC with $V_{in} = -121\text{mV}$

	Count
7350	4
7354	3
7356	3
7357	6
7358	23
7360	2565
7361	535
7362	462
7364	244
7365	650
7366	224
7368	2361
7369	830
7370	2720
7372	656
7373	14
7374	2142
7375	1
7376	2608
7377	703
7378	2297
7380	1578
7381	25
7382	3433
7383	21
7384	3673
7385	1306
7386	3687
7388	501
7389	1
7390	6410
7391	78
7392	4260
7393	1143
7394	1669
7396	1822
7397	1877
7398	13404
7402	134
7404	4
7406	3797
7407	38
7408	2375
7409	1769
7410	2421
7412	2156
7413	1667
7414	682

Table C.8: Sampled words from the pressure measurement ADC with Pressure sensor at the input

Appendix D

PCB

D.1 PCB Schematic

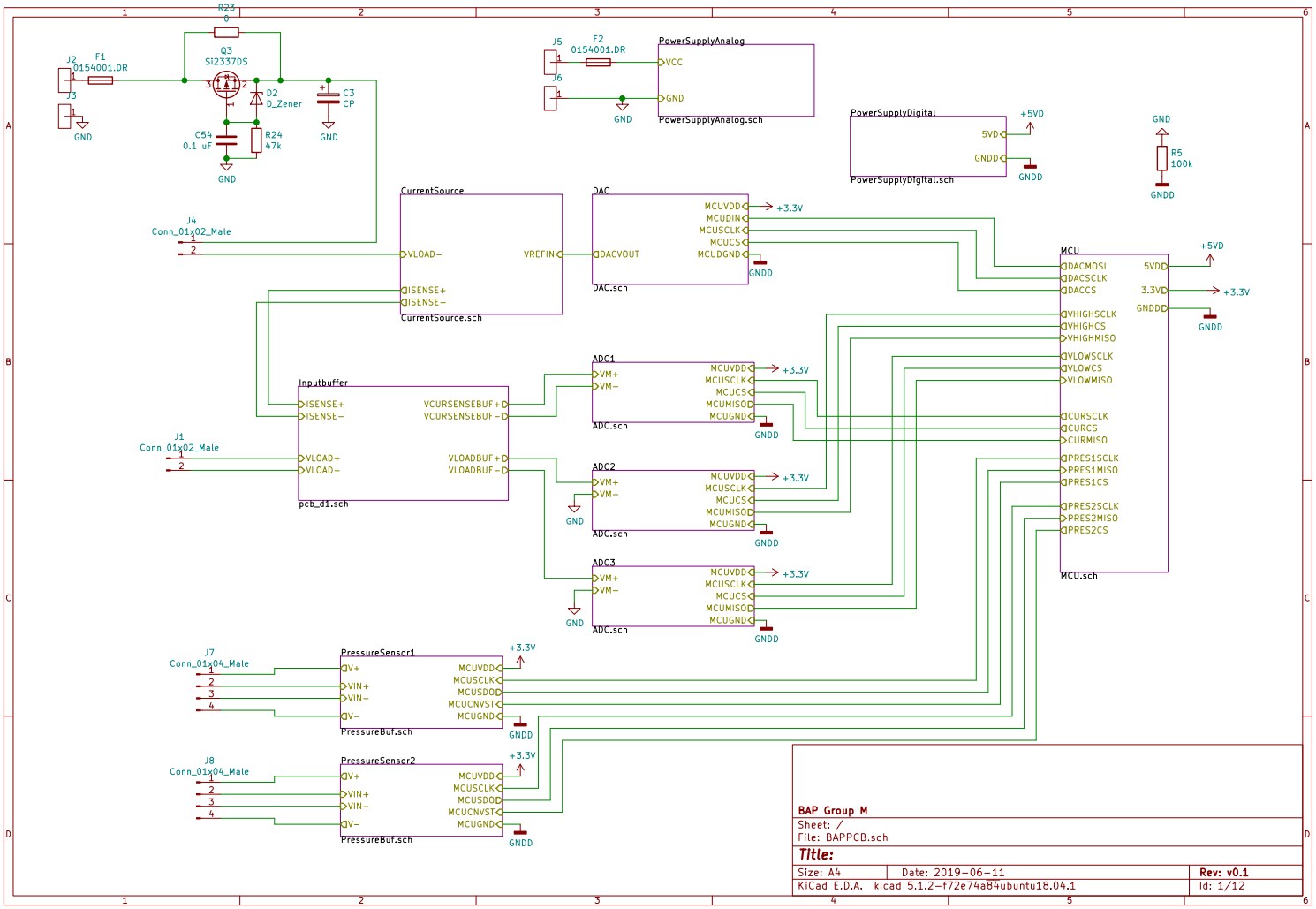
R23
0
J2
F1
0154001.DR
J3
Q3
SI2337DS
D2
D_Zener
C3
CP
C54
0.1 uF
R24
47k
GND
J5
F2
0154001.DR
J6
PowerSupplyAnalog
VCC
GND
PowerSupplyAnalog.sch
PowerSupplyDigital
5VD
GNDD
+5VD
PowerSupplyDigital.sch
R5
100k
J4
Conn_01x02_Male
CurrentSource
VLOAD−
ISENSE+
ISENSE−
VREFIN
CurrentSource.sch
DAC
DACVOUT
MCUVDD
MCUDIN
MCUSCLK
MCUCS
MCUDGND
+3.3V
DAC.sch
MCU
DACMOSI
DACSCLK
DACCS
5VDD
3.3VD
VHIGHSCLK
VHIGHCS
VHIGHMISO
VLOWSCLK
VLOWCS
VLOWMISO
CURSCLK
CURCS
CURMISO
PRES1SCLK
PRES1MISO
PRES1CS
PRES2SCLK
PRES2MISO
PRES2CS
MCU.sch
Inputbuffer
VCURSENSEBUF+
VCURSENSEBUF−
VLOADBUF+
VLOADBUF−
J1
Conn_01x02_Male
pcb_d1.sch
ADC1
ADC2
ADC3
VM+
VM−
MCUSCLK
MCUCS
MCUMISO
MCUGND
ADC.sch
J7
Conn_01x04_Male
PressureSensor1
V+
VIN+
VIN−
V−
MCUSDOD
MCUCNVST
PressureBuf.sch
J8
Conn_01x04_Male
PressureSensor2
BAP Group M
Sheet: /
File: BAPPCB.sch
Title:
Size: A4
Date: 2019−06−11
Rev: v0.1
KiCad E.D.A. kicad 5.1.2−f72e74a84ubuntu18.04.1
Id: 1/12

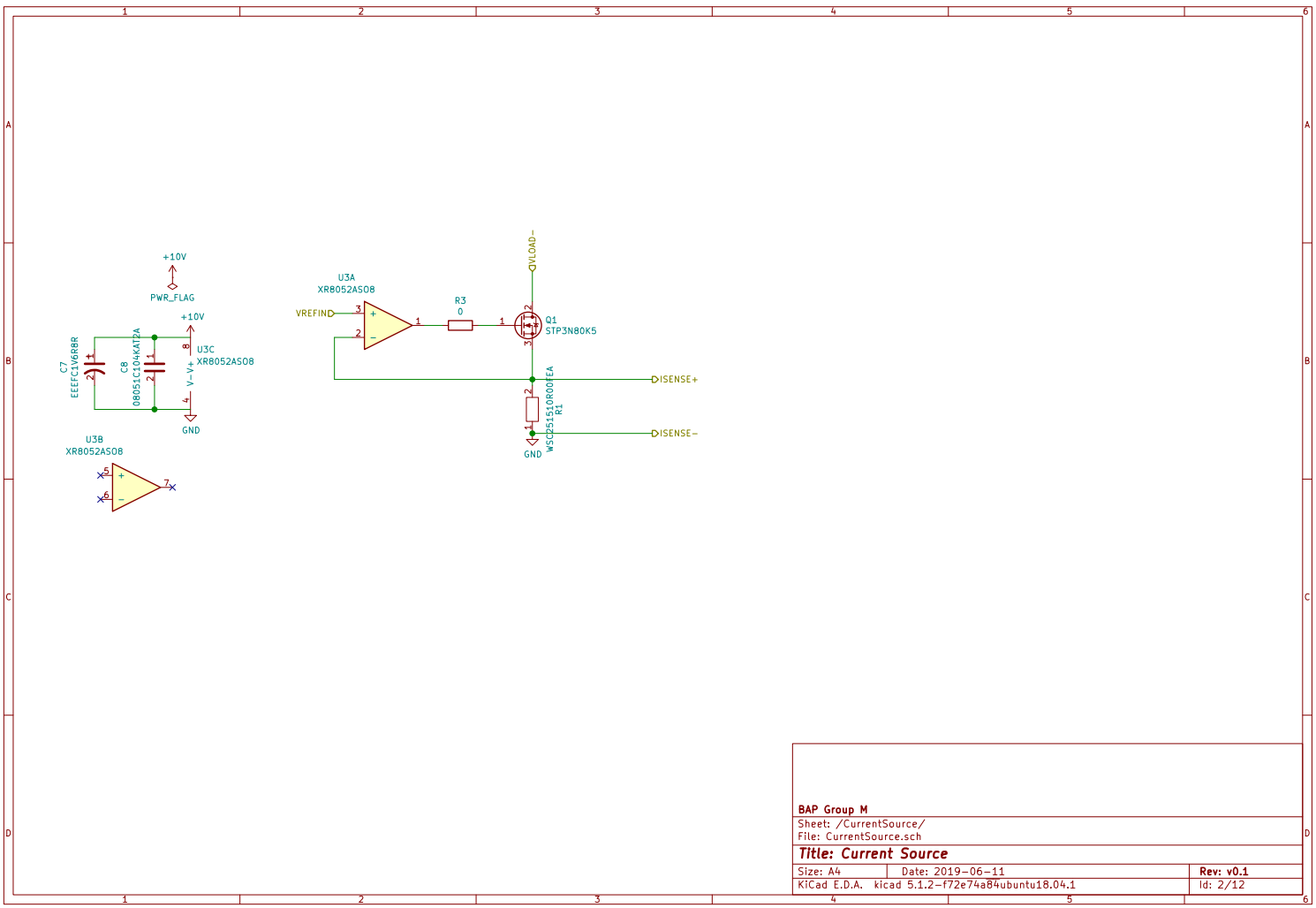
+10V
PWR_FLAG
+10V
U3C
XR8052ASO8
V-
V+
GND
C7
EEEFC1V6R8R
C8
08051C104KAT2A
U3B
XR8052ASO8
U3A
XR8052ASO8
VREFIN
R3
0
Q1
STP3N80K5
VLOAD-
ISENSE+
ISENSE-
R1
WSC2515ROR00FEA
GND
BAP Group M
Sheet: /CurrentSource/
File: CurrentSource.sch
Title: Current Source
Size: A4
Date: 2019-06-11
Rev: v0.1
KiCad E.D.A. kicad 5.1.2-f72e74a84ubuntu18.04.1
Id: 2/12

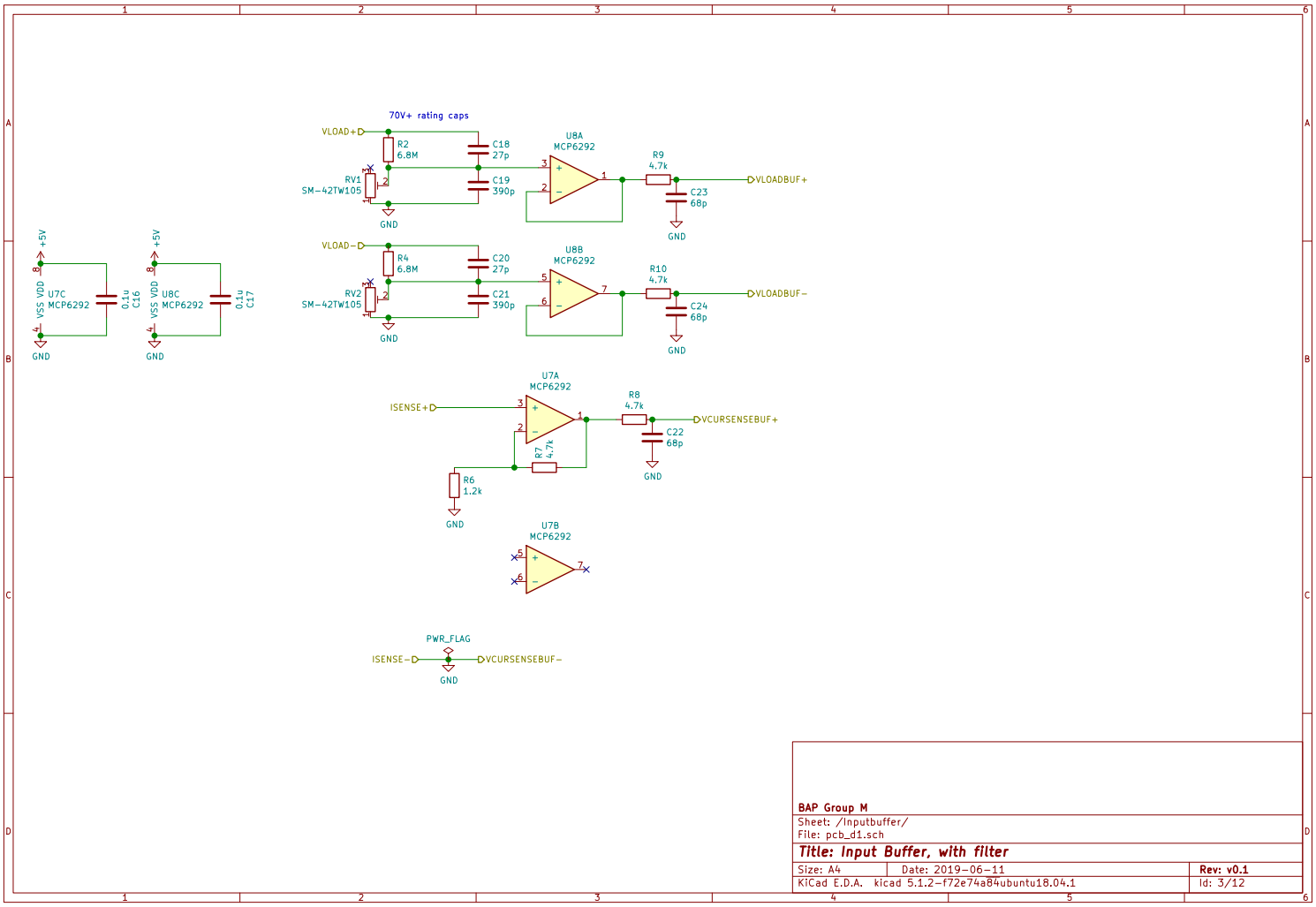
70V+ rating caps
VLOAD+
R2
6.8M
RV1
SM-42TW105
C18
27p
C19
390p
U8A
MCP6292
R9
4.7k
C23
68p
VLOADBUF+
VLOAD-
R4
6.8M
RV2
SM-42TW105
C20
27p
C21
390p
U8B
MCP6292
R10
4.7k
C24
68p
VLOADBUF-
U7C
MCP6292
U8C
MCP6292
0.1u
C16
0.1u
C17
+5V
VSS
VDD
GND
U7A
MCP6292
ISENSE+
R8
4.7k
C22
68p
VCURSENSEBUF+
R7
4.7k
R6
1.2k
U7B
MCP6292
PWR_FLAG
ISENSE-
VCURSENSEBUF-
BAP Group M
Sheet: /Inputbuffer/
File: pcb_d1.sch
Title: Input Buffer, with filter
Size: A4
Date: 2019-06-11
Rev: v0.1
KiCad E.D.A. kicad 5.1.2-f72e74a84ubuntu18.04.1
Id: 3/12

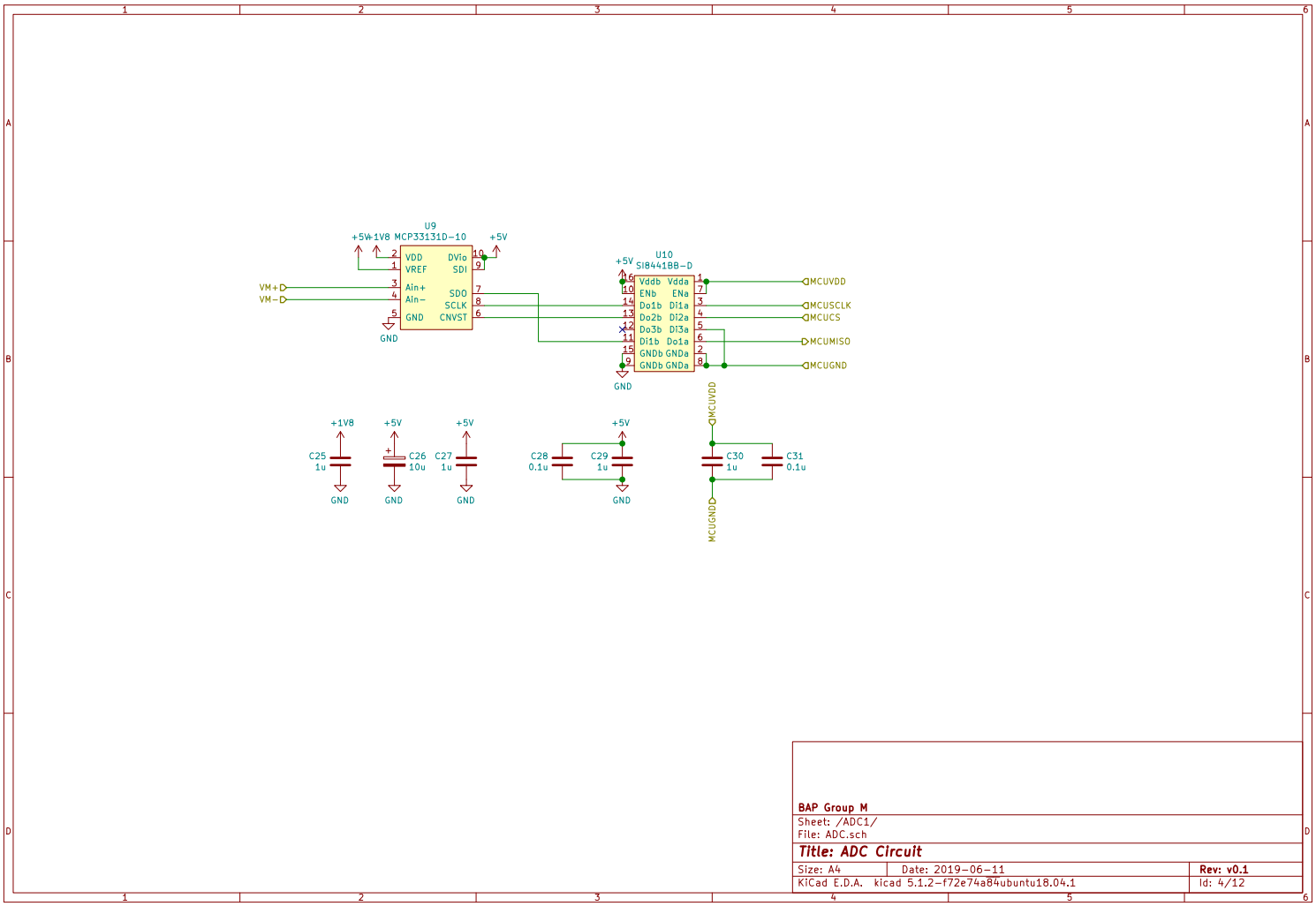
U9
MCP33131D-10
+5V
+1V8
VDD
VREF
Ain+
Ain-
GND
DVio
SDI
SDO
SCLK
CNVST
VM+
VM-
U10
SI8441BB-D
Vddb
ENb
Do1b
Do2b
Do3b
Di1b
GNDb
Vdda
ENa
Di1a
Di2a
Di3a
Do1a
GNDa
MCUVDD
MCUSCLK
MCUCS
MCUMISO
MCUGND
C25
1u
C26
10u
C27
1u
C28
0.1u
C29
1u
C30
1u
C31
0.1u
BAP Group M
Sheet: /ADC1/
File: ADC.sch
Title: ADC Circuit
Size: A4
Date: 2019-06-11
Rev: v0.1
KiCad E.D.A. kicad 5.1.2-f72e74a84ubuntu18.04.1
Id: 4/12

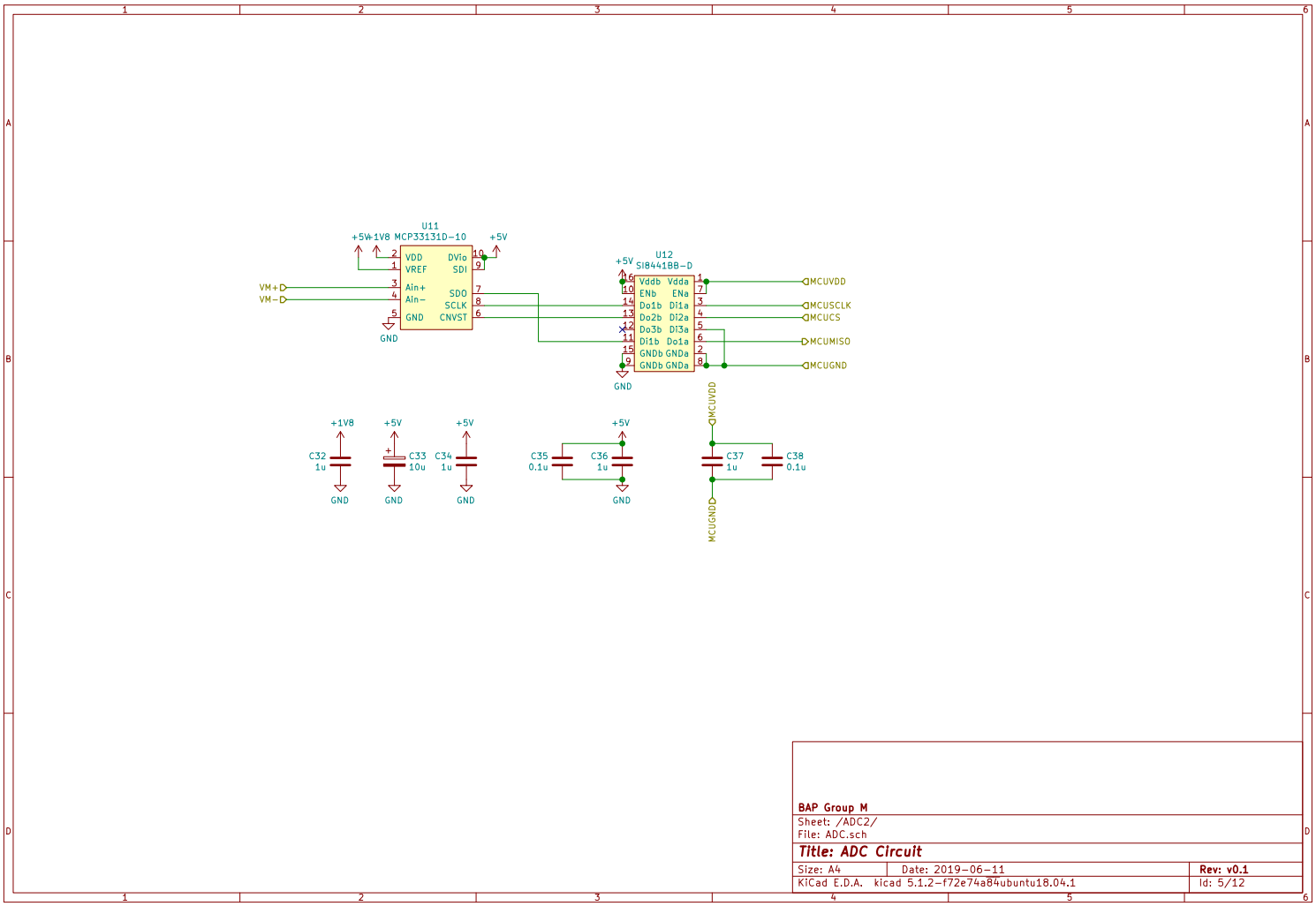
U11
MCP33131D-10
+5V
+1V8
VDD
VREF
Ain+
Ain-
GND
DVio
SDI
SDO
SCLK
CNVST
VM+
VM-
U12
SI8441BB-D
Vddb
ENb
Do1b
Do2b
Do3b
Di1b
GNDb
Vdda
ENa
Di1a
Di2a
Di3a
Do1a
GNDa
MCUVDD
MCUSCLK
MCUCS
MCUMISO
MCUGND
C32
1u
C33
10u
C34
1u
C35
0.1u
C36
1u
C37
1u
C38
0.1u
BAP Group M
Sheet: /ADC2/
File: ADC.sch
Title: ADC Circuit
Size: A4
Date: 2019-06-11
Rev: v0.1
KiCad E.D.A. kicad 5.1.2-f72e74a84ubuntu18.04.1
Id: 5/12

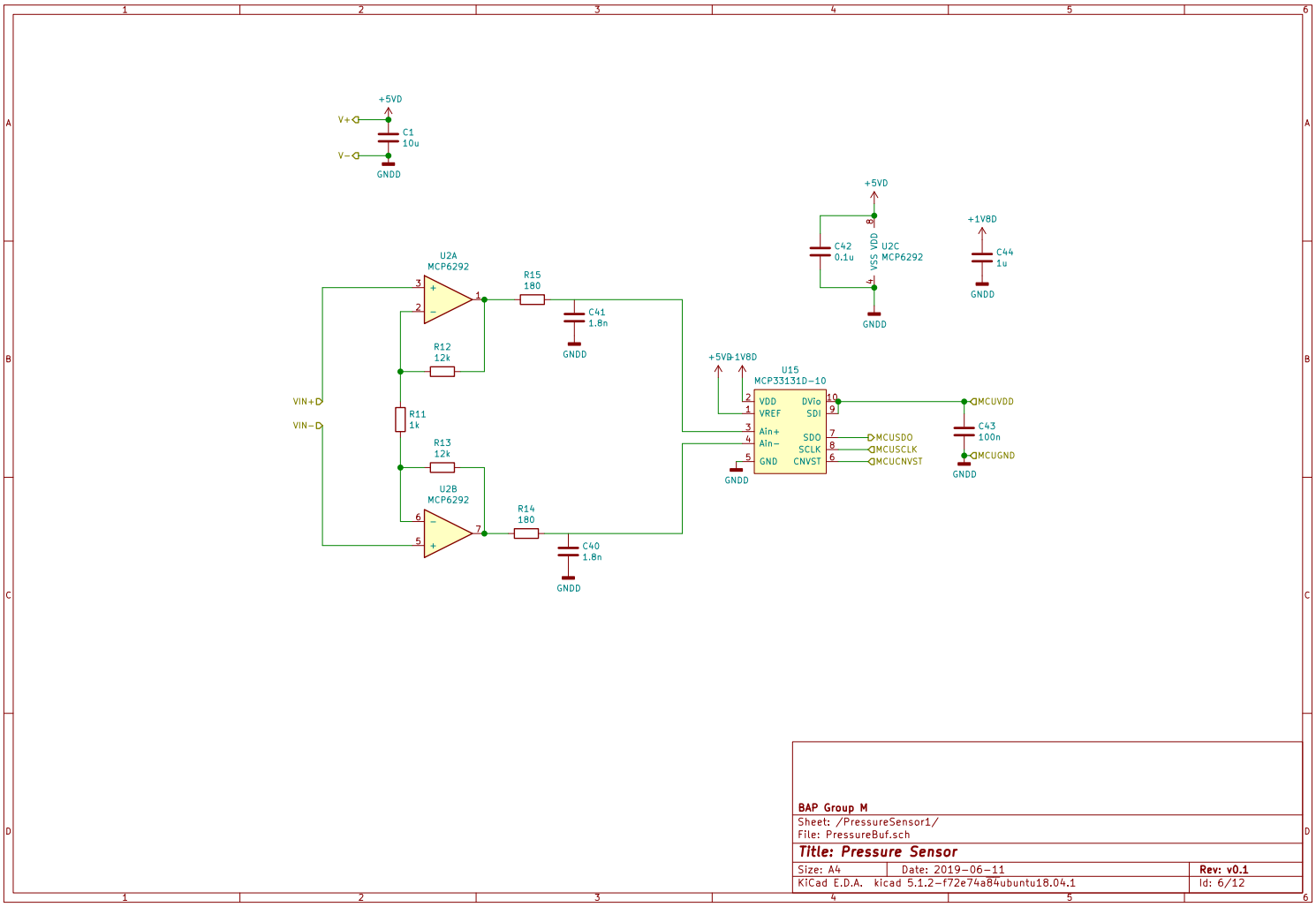
+5VD
V+
C1
10u
V-
GNDD
U2A
MCP6292
R15
180
C41
1.8n
R12
12k
R11
1k
R13
12k
U2B
MCP6292
R14
180
C40
1.8n
VIN+
VIN-
+5VD
C42
0.1u
U2C
MCP6292
+1V8D
C44
1u
U15
MCP33131D-10
VDD
VREF
Ain+
Ain-
GND
DVio
SDI
SDO
SCLK
CNVST
MCUSDO
MCUSCLK
MCUCNVST
MCUVDD
C43
100n
MCUGND
BAP Group M
Sheet: /PressureSensor1/
File: PressureBuf.sch
Title: Pressure Sensor
Size: A4
Date: 2019-06-11
Rev: v0.1
KiCad E.D.A. kicad 5.1.2-f72e74a84ubuntu18.04.1
Id: 6/12

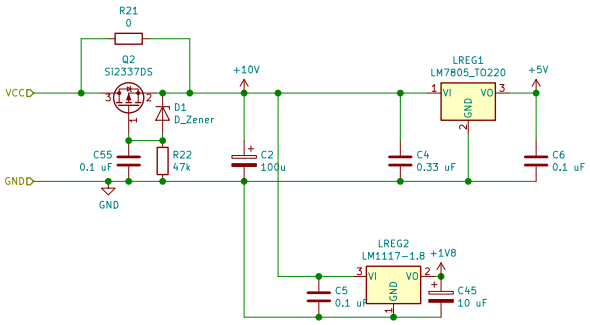

BAP Group M

Sheet: /PowerSupplyAnalog/

File: PowerSupplyAnalog.sch

Title: Analog Power Supply

Size: A4	Date: 2019-06-11	**Rev: v0.1**
KiCad E.D.A. kicad 5.1.2-f72e74a84ubuntu18.04.1		Id: 7/12

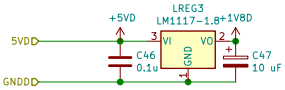

BAP Group M

Sheet: /PowerSupplyDigital/

File: PowerSupplyDigital.sch

Title: Digital Power Supply

Size: A4	Date: 2019-06-11	**Rev: v0.1**
KiCad E.D.A. kicad 5.1.2-f72e74a84ubuntu18.04.1		Id: 8/12

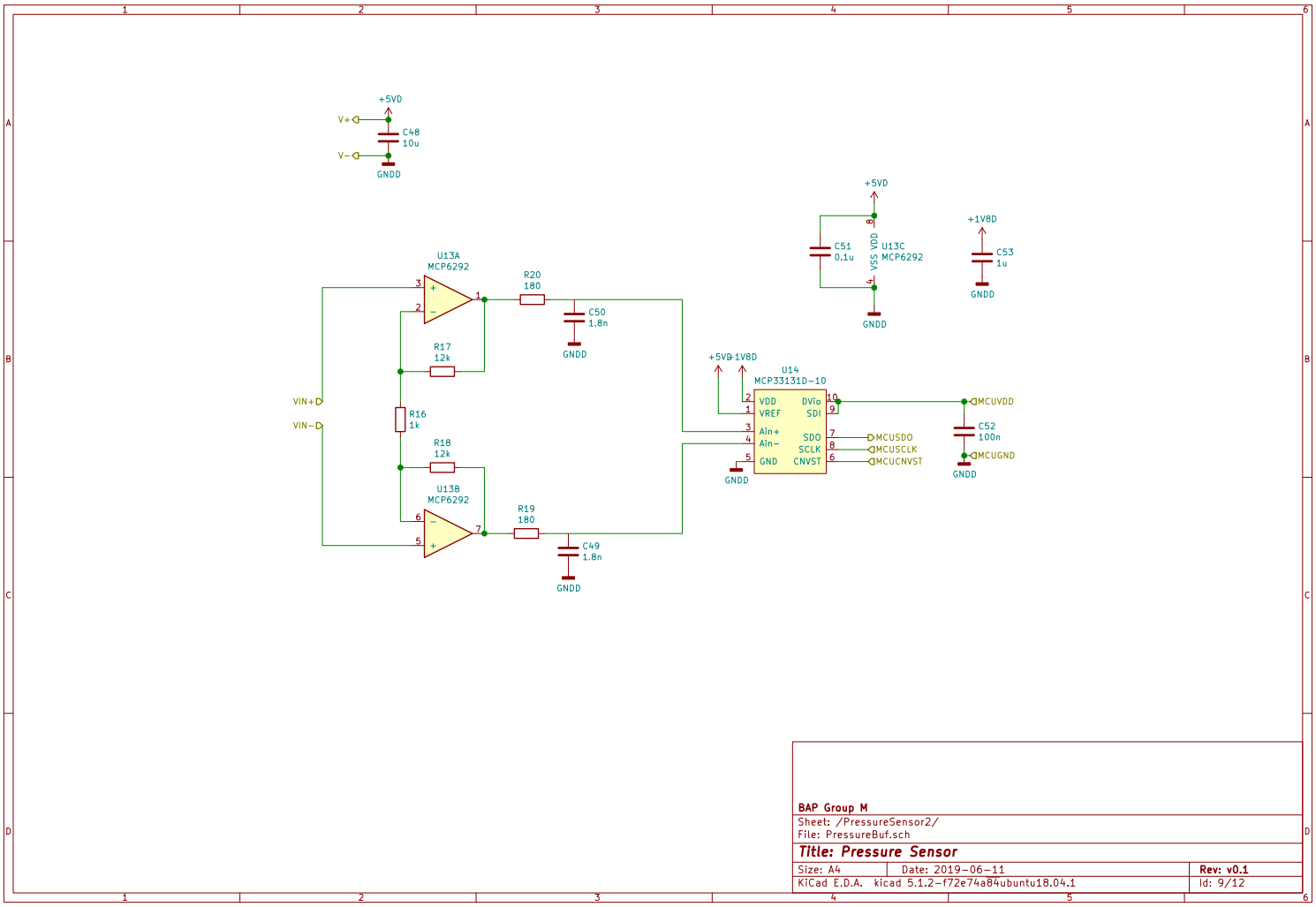
+5VD
V+
C48
10u
V-
GNDD
U13A
MCP6292
R20
180
C50
1.8n
R17
12k
VIN+
R16
1k
VIN-
R18
12k
U13B
MCP6292
R19
180
C49
1.8n
+5VD
C51
0.1u
U13C
MCP6292
+1V8D
C53
1u
U14
MCP33131D-10
VDD
VREF
Ain+
Ain-
GND
DVio
SDI
SDO
SCLK
CNVST
MCUSDO
MCUSCLK
MCUCNVST
MCUVDD
C52
100n
MCUGND
BAP Group M
Sheet: /PressureSensor2/
File: PressureBuf.sch
Title: Pressure Sensor
Size: A4
Date: 2019-06-11
Rev: v0.1
KiCad E.D.A. kicad 5.1.2-f72e74a84ubuntu18.04.1
Id: 9/12

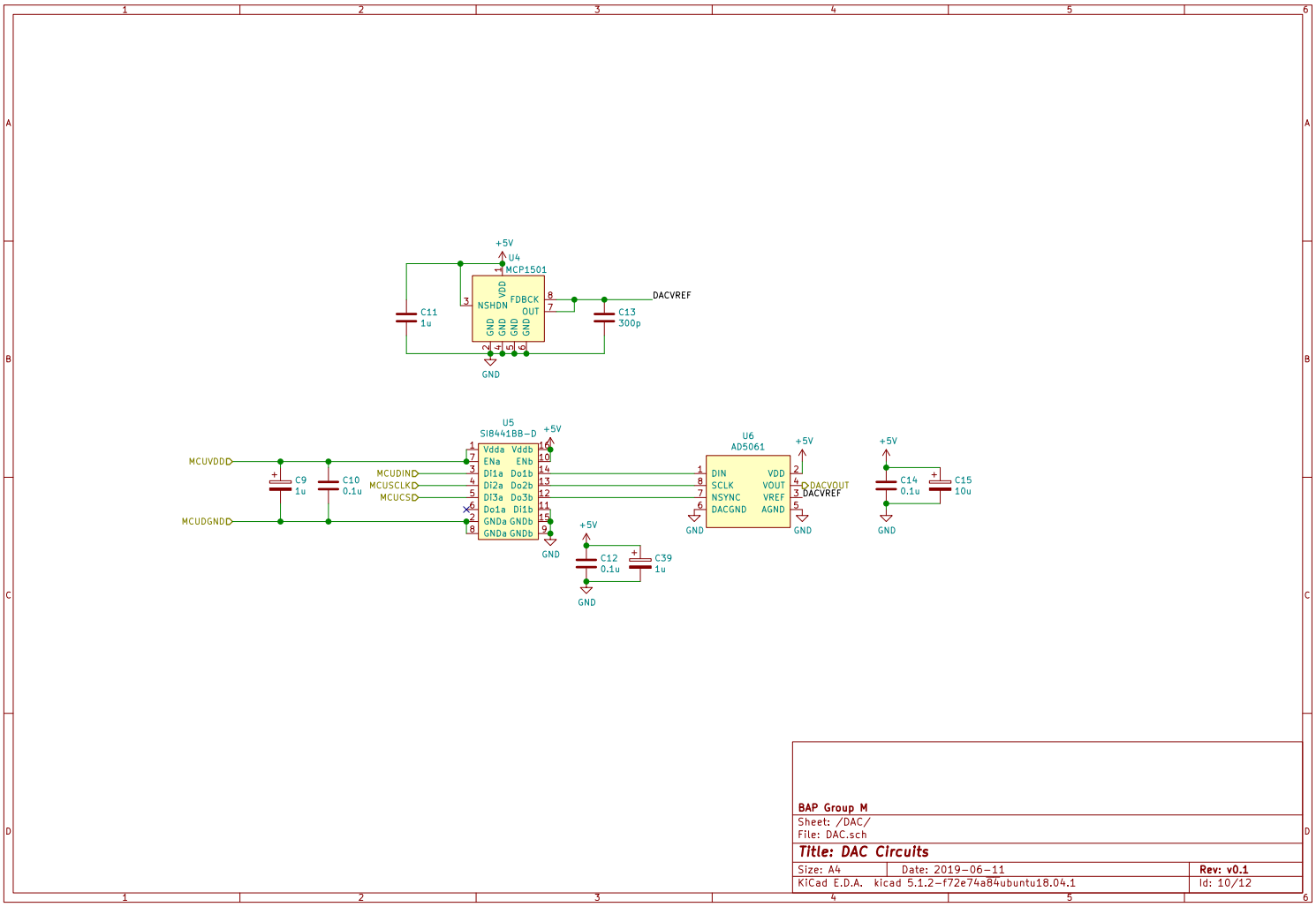
+5V
U4
MCP1501
VDD
NSHDN
FDBCK
OUT
GND
GND
GND
GND
C11
1u
C13
300p
DACVREF
GND
U5
SI8441BB-D
Vdda Vddb
ENa ENb
DI1a Do1b
DI2a Do2b
DI3a Do3b
Do1a DI1b
GNDa GNDb
GNDa GNDb
MCUVDD
MCUDGND
MCUDIN
MCUSCLK
MCUCS
C9
1u
C10
0.1u
C12
0.1u
C39
1u
U6
AD5061
DIN
SCLK
NSYNC
DACGND
VDD
VOUT
VREF
AGND
DACVOUT
DACVREF
C14
0.1u
C15
10u
BAP Group M
Sheet: /DAC/
File: DAC.sch
Title: DAC Circuits
Size: A4
Date: 2019-06-11
Rev: v0.1
KiCad E.D.A. kicad 5.1.2-f72e74a84ubuntu18.04.1
Id: 10/12

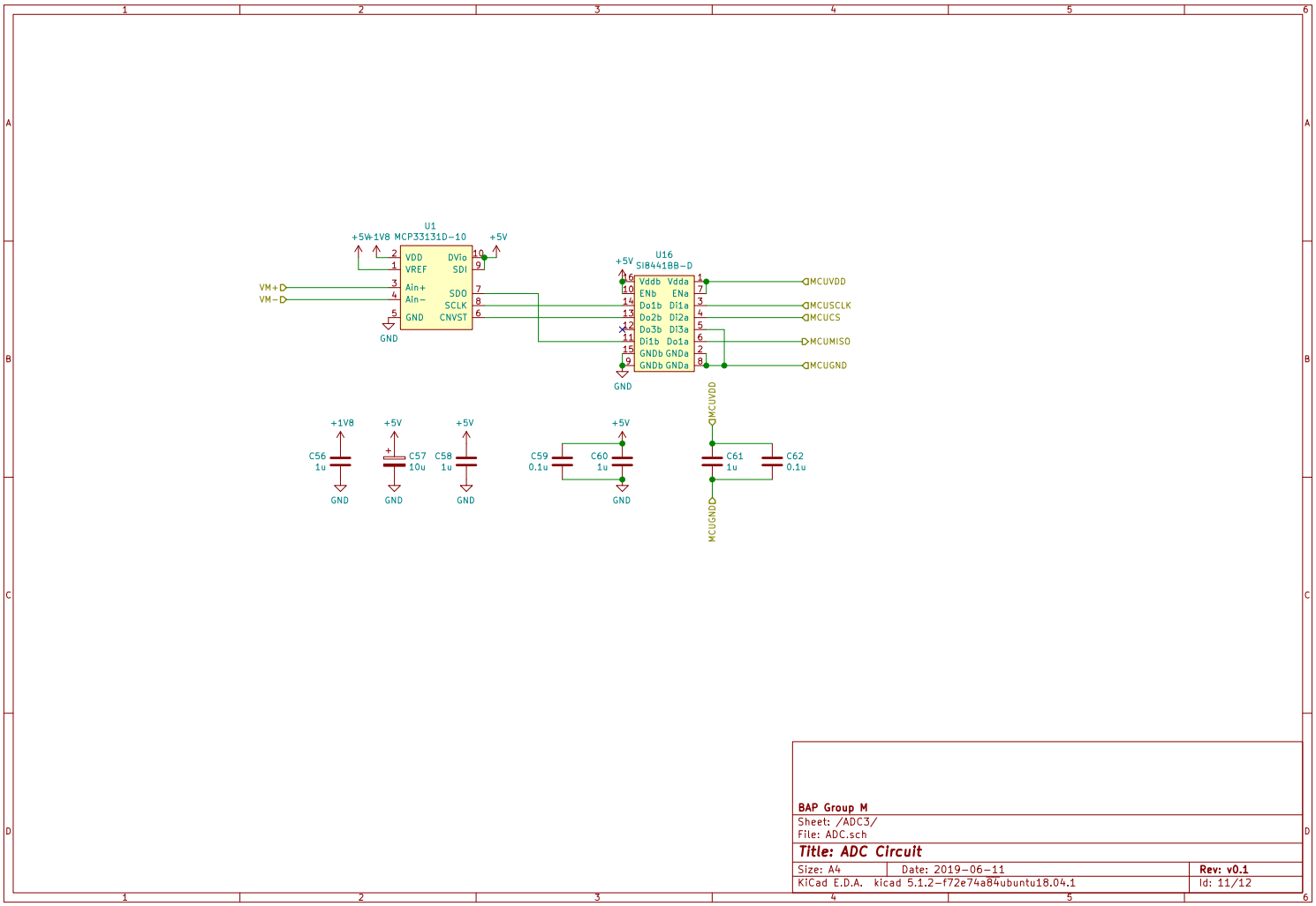
U1
MCP33131D-10
+5V
+1V8
VDD
VREF
Ain+
Ain-
GND
DVio
SDI
SDO
SCLK
CNVST
VM+
VM-
U16
SI8441BB-D
Vddb
ENb
Do1b
Do2b
Do3b
Di1b
GNDb
Vdda
ENa
Di1a
Di2a
Di3a
Do1a
GNDa
MCUVDD
MCUSCLK
MCUCS
MCUMISO
MCUGND
C56
1u
C57
10u
C58
1u
C59
0.1u
C60
1u
C61
1u
C62
0.1u
MCUGNDD
BAP Group M
Sheet: /ADC3/
File: ADC.sch
Title: ADC Circuit
Size: A4
Date: 2019-06-11
Rev: v0.1
KiCad E.D.A. kicad 5.1.2-f72e74a84ubuntu18.04.1
Id: 11/12

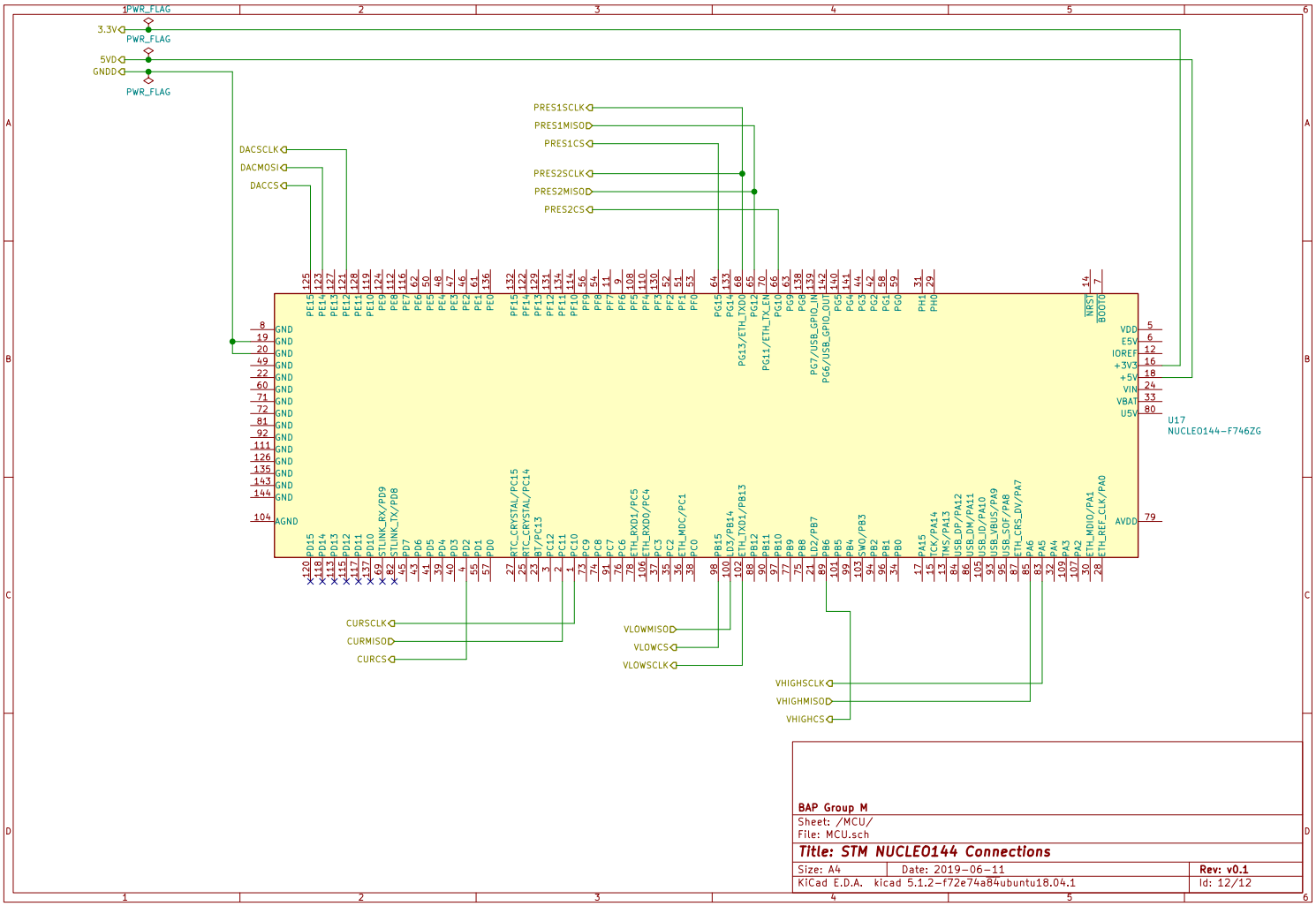
PWR_FLAG
3.3V
PWR_FLAG
5VD
GNDD
PWR_FLAG
DACSCLK
DACMOSI
DACCS
PRES1SCLK
PRES1MISO
PRES1CS
PRES2SCLK
PRES2MISO
PRES2CS
U17
NUCLEO144-F746ZG
CURSCLK
CURMISO
CURCS
VLOWMISO
VLOWCS
VLOWSCLK
VHIGHSCLK
VHIGHMISO
VHIGHCS
BAP Group M
Sheet: /MCU/
File: MCU.sch
Title: STM NUCLEO144 Connections
Size: A4
Date: 2019-06-11
Rev: v0.1
KiCad E.D.A. kicad 5.1.2-f72e74a84ubuntu18.04.1
Id: 12/12

D.2 PCB Layers

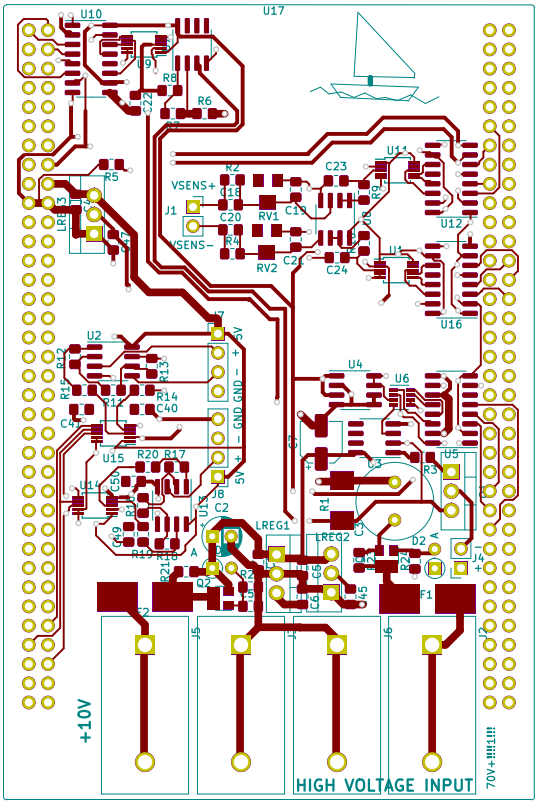

Figure D.1: Front of the PCB with Copper Layer, Silkscreen and Mounting Holes

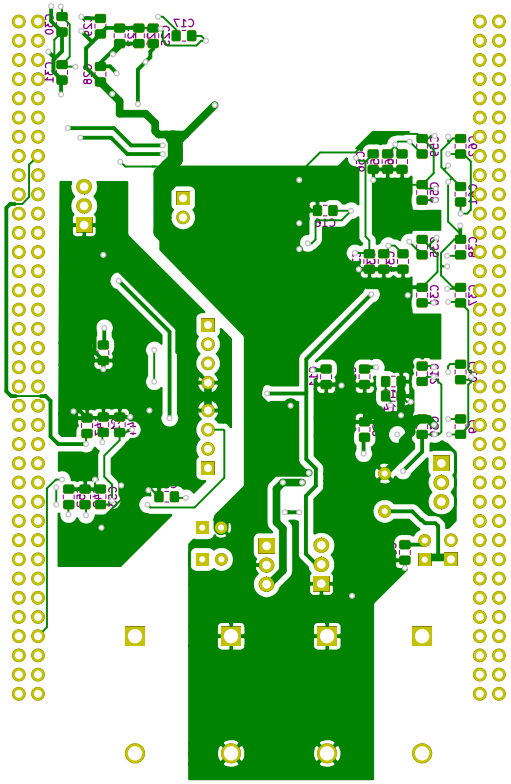

Figure D.2: Back of the PCB with Copper Layer, Silkscreen and Mounting Holes

D.3 PCB result

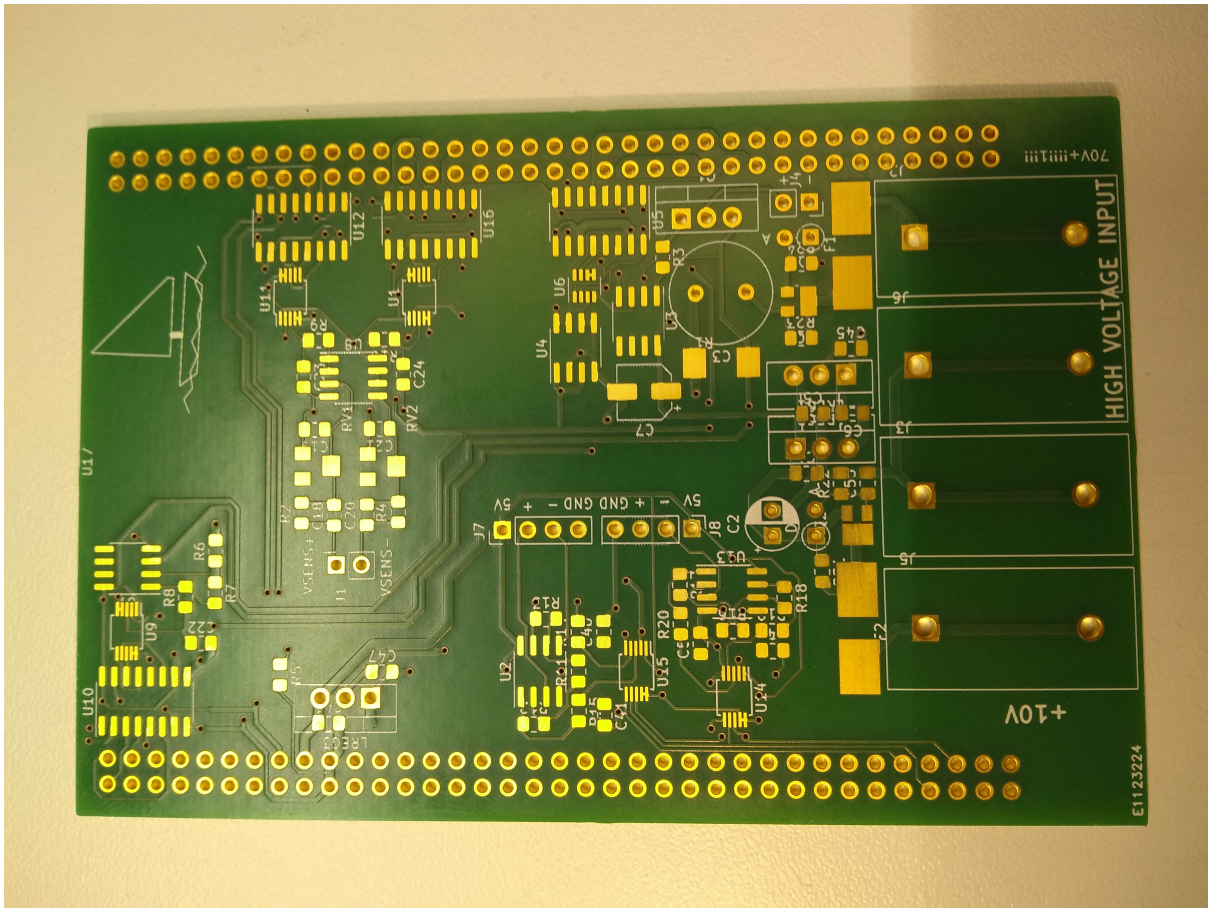

Figure D.3: Front of the PCB

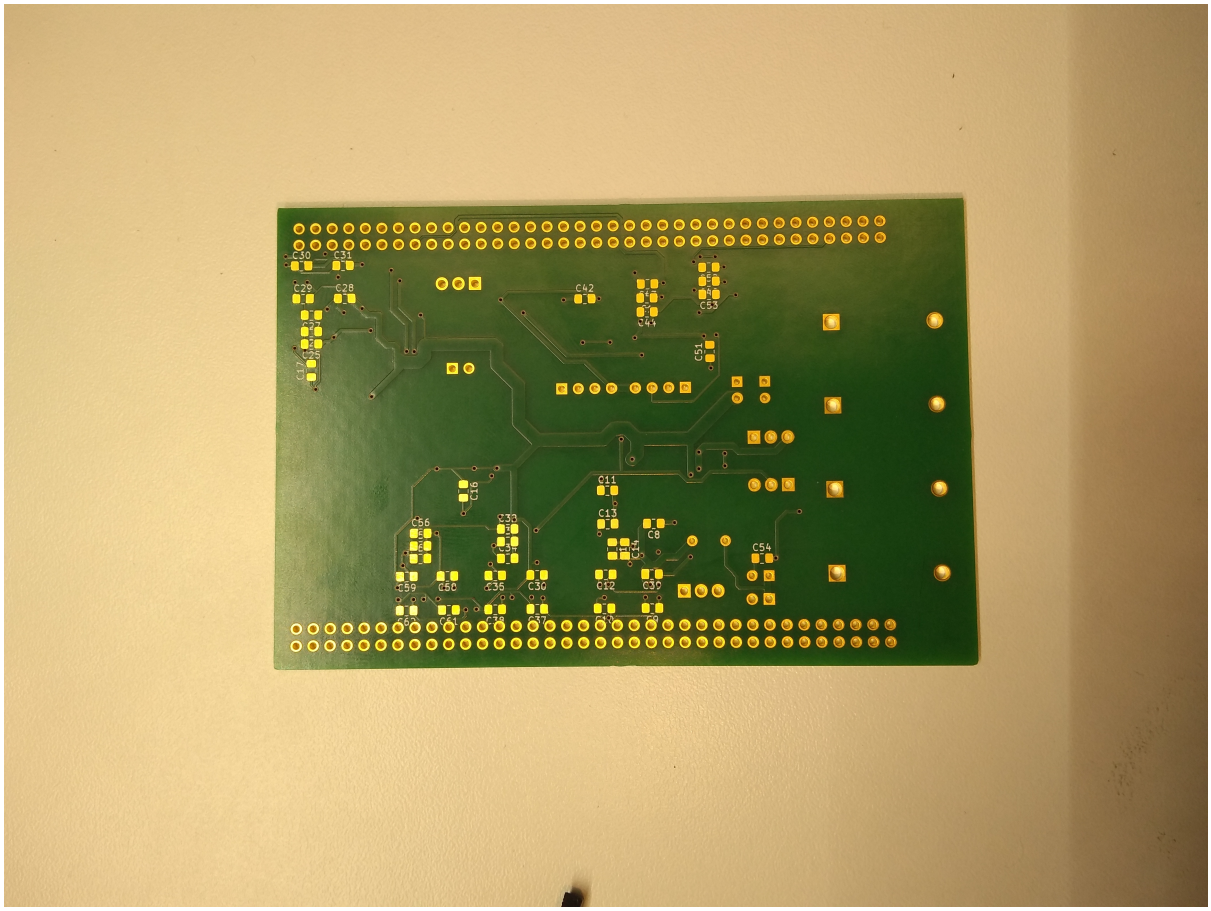

Figure D.4: Back of the PCB